The dynamics of elliptically shaped regions of uniform vorticity in time-periodic, linear external velocity fields

1995 Fluid Dyn. Res. 15 205

(http://iopscience.iop.org/1873-7005/15/4/A01)

ELSEVIER

Fluid Dynamics Research 15 (1995) 205–235

FLUID DYNAMICS RESEARCH

The dynamics of elliptically shaped regions of uniform vorticity in time-periodic, linear external velocity fields

Kayo Ide[1] and Stephen Wiggins[2]

Climate Dynamics Center, Institute of Geophysics and Planetary Physics, University of California, Los Angeles, Los Angeles, CA 90024-1567, USA

Applied Mechanics 104-44, Caltech, Pasadena, CA 91125, USA

Received 9 April 1993; revised 25 July 1994

Abstract

In this paper we extend results of Kida (J. Phys. Soc. Japan 50 (1981) 3517) and Neu (Phys. Fluids 27 (1984) 2397) on the dynamics of elliptically shaped regions of uniform vorticity in external linear velocity fields. The work of Kida and Neu was concerned with time-independent external linear velocity fields and we consider the case in which the linear external linear velocity fields may be time-periodic. We derive a Hamiltonian formulation for such problems in such a way that a study of the problem can be reduced to the study of a two-dimensional, area preserving Poincaré map. In this way techniques from dynamical systems theory such as KAM theory and the subharmonic and homoclinic Melnikov methods can be used. With these techniques we show the existence of a variety of new solutions to the two-dimensional Euler equations on an unbounded domain; these include vortex motions that are temporally quasiperiodic, in subharmonic resonance with the linear external velocity field, and chaotic in the sense of Smale horseshoes. We give physical interpretations of these motions in terms of exchanges of energy between different components of the total excess kinetic energy of the flow field.

1 Introduction

In two-dimensional incompressible inviscid flow, the vorticity distribution completely determines the flow field as described by the Biot-Savart law (Batchelor, 1968; Saffman and Baker, 1979). Hence, a fundamental understanding of vortex dynamics (or equivalently vortex interaction process) is important for understanding the flow dynamics. There are many flows which can be modeled by a single or multiple number of discrete vortices (see, e.g., Roshko, 1976; Jimenez, 1987;

[1] This research was partially supported by NSF grant ATM90-13217 and ONR grant N0014-89-J-1845.

[2] This research was partially supported by an NSF Presidential Young Investigator Award and ONR Young Investigator Award.

SSDI 0169-5983(94)00030-1

McWilliams, 1984; Moore and Saffman 1975; Saffman and Schatzman, 1982). If the vortices are far apart (so that vortex merger does not occur), one can study the dynamics of the vortices from the point of view of deformations of individual vortices around their centroids through the influence of itself and the other vortices.

In a Lagrangian frame which translates with and rotates around a vortex blob centroid, the vortex blob configuration is changed by the influence of the self-induced velocity field and the external flow field, i.e., the local fluid particle velocity relative to the centroid. The first order approximation to the external flow field is a linear flow field around the centroid which is composed of straining and rotational effects. The straining flow field is described by two parameters, (γ, α), where γ is the strength of the straining effect and α is the inclination of the straining axis with respect to the Lagrangian coordinate frame. The straining flow field, which is irrotational, is caused by vortex interaction with other vortices and boundaries. The rotational flow, or background vorticity effect, is described by a parameter ω_R and is strictly due to the rotation of the Lagrangian frame around the centroid, because of assumptions on the discrete vortex. In this paper, we are concerned with vortex motion in an arbitrary external linear flow field. We consider elliptical regions of uniform vorticity distribution (uniform elliptical vortex, referred to as a "UEV" henceforth).

1.1. Historical background

The dynamics of a UEV in no external flow field were first formulated by Kirchoff (1876) who found that a UEV of any aspect ratio (i.e., ratio of semi-major to semi-minor axes) rotates around its centroid with a constant angular velocity, while preserving its aspect ratio (see also Lamb, 1932). Moore and Saffman (1971) showed that in a steady pure straining field, or in a steady simple shear flow, there exist steady UEV configurations. For a UEV in a steady, pure straining field, the steady UEV configuration exists with its semi-major axis aligned at an angle α of $\pi/4$ to the straining axis as long as the ratio of the straining γ and the UEV vorticity rate ω_E, i.e., γ/ω_E, is less than 0.15. For a UEV in a steady simple shear flow, the steady UEV configuration exists as long as the shear γ' and the UEV vorticity rates, i.e., γ'/ω_E, are less than 0.21.

The equations for the UEV motion in steady external linear flow fields were first obtained by Kida (1981) as a set of two dimensional ordinary differential equations for (η, θ), where η is the aspect ratio of the ellipse, and θ is the inclination angle of the semi-major axis of the ellipse with respect to the Lagrangian coordinate frame. The solutions of Kida's equations correspond to exact solutions of Euler equations. Kida also gave a bifurcation diagram in terms of the parameters $(\omega_R/\omega_E, \gamma/\omega_E)$ that described the possible solutions to his equations, where $\omega_R = 2(\gamma + \gamma')$. Neu (1984) reformulated the equations for the UEV motion as a Hamiltonian system. However, the transformation to the Hamiltonian system that Neu adopted involves scaling of the time variable by $(\eta^2 - 1)/\eta$, which means that the solutions given in the Hamiltonian system do not correspond to the UEV motion in a time-wise sense. This becomes a significant obstacle when we consider the UEV motion in time dependent external linear flow fields. Related work that considers the dynamics of UEV's in time-periodic strain rate fields can be found in Bertozzi (1988), although this work is in a non-Hamiltonian setting.

This paper is outlined as follows, in Section 2 we show that Kida's equations for the UEV motion hold in any time dependent external linear flow field described by three variables $(\gamma(t), \alpha(t), \omega_R(t))$

In order to facilitate techniques form dynamical systems theory, we transform the equations for the UEV motion into Hamiltonian from (see Melander et al., 1987) in such a way that time is not rescaled by the dependent variables. In Section 3 we recover the bifurcation diagram given by Kida, and give a complete phase plane analysis showing all possible solutions. We then described these motions in terms of energy transfer. In Section 4 we consider the motion of UEV's in unsteady external linear flow fields. In this case fundamentally new types of dynamics are possible; including chaotic motion of the vortex boundary as well as transitions between oscillating, rotating, and elongating motions.

2. Coordinates and equations of motion

We consider a UEV whose centroid is located at the origin of the Lagrangian frame denoted by (x, y) with $z = x + iy$. The semi-major axis, a, a semi-minor axis, b, of the ellipse define a UEV fixed coordinate system denoted by (X, Y) with $Z = X + iY$. The angle, θ, between the semi-major axis and the x-axis is referred to as the inclination (or tilting) angle of the UEV and provides the relation between two coordinate systems (x, y) and (X, Y) as follows

$$\boldsymbol{x} = R(\theta)\boldsymbol{X} \qquad z = e^{i\theta} Z, \tag{1}$$

where

$$\boldsymbol{x} = \begin{pmatrix} x \\ y \end{pmatrix}, \quad \boldsymbol{X} = \begin{pmatrix} X \\ Y \end{pmatrix}, \quad R(\theta) = \begin{pmatrix} \cos\theta & -\sin\theta \\ \sin\theta & \cos\theta \end{pmatrix}.$$

In Fig. 1 we illustrate the coordinates.

The ratio $\eta = a/b$ is referred to as the *aspect ratio* of a UEV and is, by definition, greater than unity. We note that the values $\eta = 1, \infty$ correspond to a uniform circular vortex (Rankine vortex) and a vortex sheet, respectively. The area of the UEV $A = \pi ab$ and the total circulation $\Gamma = \omega_E A$ are invariants in the flow where the subscript "E" refers to ellipse. We define the mean core radius,

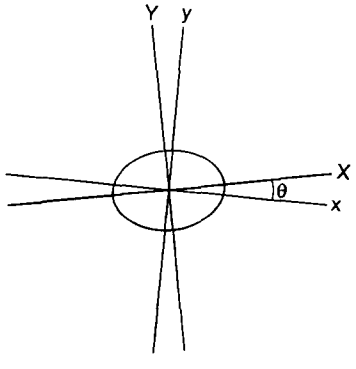

Fig. 1. Coordinates associated with a UEV.

Λ, of a UEV to be the radius of a circle with center at the center of the UEV that encloses a region of area A, i.e., $A = \pi\Lambda^2$. The UEV configuration is uniquely defined by (η, θ) for $\eta \geqslant 1$ and $0 \leqslant \theta < \pi$.

Now we want to give a brief account of the derivation of the equations of motion of a UEV. As mentioned earlier, a derivation of the equations for UEV's in constant linear velocity fields can be found in Kida (1981) and Neu (1984). Here we will merely outline the steps and point out the place in the derivation where it is apparent that the external, linear velocity field may be time dependent.

Any linear external flow field can always be decomposed into two components i.e., strain and rotation, that are described by three parameters $(\gamma, \alpha, \omega_R)$ where γ is rate of strain acting along the strain axis ($x_s - y_s$ in Fig. 2) with rotation angle α with respect to the Lagrangian axis ($x - y$), and ω_R is the rotation rate. In Fig. 2 we illustrate the streamlines (assuming γ, α and ω_R constant) induced by these two velocity fields individually.

The velocity field inside the UEV is the sum of the velocity field due to the elliptical vortex distribution and the linear velocity field and has the form

$$\dot{\boldsymbol{x}} = \dot{\boldsymbol{x}}_E + \dot{\boldsymbol{x}}_S + \dot{\boldsymbol{x}}_R = U(\eta, \theta; \omega_E; \gamma, \alpha, \omega_R)\boldsymbol{x}, \tag{2}$$

where

$$U(\eta, \theta; \omega_E; \gamma, \alpha, \omega_R) = \frac{-\omega_E}{\eta + 1} R(\theta)\begin{pmatrix} 0 & \eta \\ -1 & 0 \end{pmatrix} R(-\theta) + \gamma R(\alpha)\begin{pmatrix} 0 & 0 \\ 0 & -1 \end{pmatrix} R(-\alpha) + \frac{\omega_R}{2}\begin{pmatrix} 0 & 1 \\ -1 & 0 \end{pmatrix} \tag{3}$$

The first term represents the velocity induced by the UEV (inside and on the boundary of the UEV), the second term represents a linear strain field, denoted by a subscript "S", and the third term represents a linear vorticity field or rotation, denoted by a subscript "R". The important feature here is that the total velocity field $\dot{\boldsymbol{x}}$ depends linearly on the space variables $\boldsymbol{x}$. *Note also that* γ, α, *and* ω_R *may be time-dependent.* Although total vorticity is an invariant in the flow, ω_R can be time-dependent by rotating the Lagrangian frame with respect to the absolute coordinate system.

The equation for the curve bounding the UEV (i.e., the equation for an ellipse) with semi-major axis inclined at an angle θ with the horizontal can be expressed as follows

$$\boldsymbol{x}^{\mathrm{T}} E(\eta, \theta; \Lambda)\boldsymbol{x} = 1, \tag{4}$$

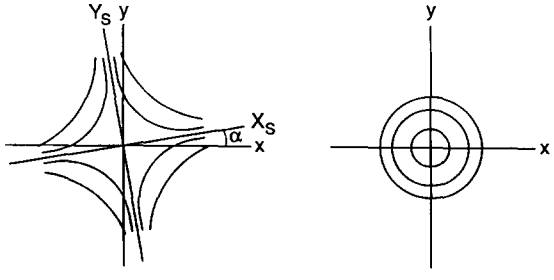

Fig. 2. Streamlines induced by the (a) linear external straining fields and (b) the linear external rotational field.

where the matrix $E(\eta, \theta; \Lambda)$ is defined by

$$E(\eta, \theta; \Lambda) = \frac{1}{\Lambda^2} R(\theta) \begin{pmatrix} 1/\eta & 0 \\ 0 & \eta \end{pmatrix} R(-\theta). \tag{5}$$

For an ideal fluid, vorticity at any point is convected by the local velocity at that point. Hence it follows that

$$\frac{\mathrm{D}}{\mathrm{D}t}(\boldsymbol{x}^{\mathrm{T}} E(\eta, \theta; \Lambda)\boldsymbol{x}) = \frac{\mathrm{D}}{\mathrm{D}t} 1 = 0, \tag{6}$$

where $\mathrm{D}/\mathrm{D}t$ is the usual material derivative. Carrying out the differentiation of (4) and substituting (2), (3), and (5) into the result gives

$$\boldsymbol{x}^{\mathrm{T}}(\dot{E} + U^{\mathrm{T}}E + EU)\boldsymbol{x} = 0, \tag{7}$$

which is satisfied by requiring

$$\dot{E} + U^{\mathrm{T}}E + EU = 0. \tag{8}$$

In (7) we see very clearly the important role played by the linearity of the velocity field in the space variables. Writing out (8) explicitly in matrix form gives the following equations

$$\frac{1}{\Lambda^2}\left[\begin{pmatrix} -\frac{\dot{\eta}}{\eta^2} & 0 \\ 0 & \dot{\eta} \end{pmatrix} + \begin{pmatrix} \frac{2p}{\eta} & q\left(\eta + \frac{1}{\eta}\right) + r\left(\eta - \frac{1}{\eta}\right) \\ q\left(\eta + \frac{1}{\eta}\right) + r\left(\eta - \frac{1}{\eta}\right) & -2p\eta \end{pmatrix} + \begin{pmatrix} 0 & -\left(\eta - \frac{1}{\eta}\right)\dot{\theta} \\ -\left(\eta - \frac{1}{\eta}\right)\dot{\theta} & 0 \end{pmatrix}\right] = 0, \tag{9}$$

where

$$p \equiv \gamma \cos 2(\theta - \alpha), \quad q \equiv -\gamma \sin 2(\theta - \alpha), \quad r \equiv \frac{\omega_E}{\eta + 1} + \frac{\omega_R}{2}.$$

We see very clearly that there are only two independent components of (9). The reason for this is that symmetry and incompressibility impose two constraints on $U^{\mathrm{T}}E + EU$. Writing out these two independent equations gives

$$\begin{pmatrix} \frac{\mathrm{d}\eta}{\mathrm{d}t} \\ \frac{\mathrm{d}\theta}{\mathrm{d}t} \end{pmatrix} = \begin{pmatrix} 2\gamma(t)\eta \cos 2[\theta - \alpha(t)] \\ \frac{\omega_E \eta}{(\eta + 1)^2} - \gamma(t)\frac{\eta^2 + 1}{\eta^2 - 1} \sin 2[\theta - \alpha(t)] + \frac{\omega_R(t)}{2} \end{pmatrix}, \tag{10}$$

where we have explicitly indicated the possible time-dependence of γ, α, and ω_R.

2.1. The Hamiltonian structure

The global analysis of the dynamics of (10) is greatly facilitated if we can put the equations in Hamiltonian form. For the case of γ, α, and ω_R constant Neu (1984) showed that by rescaling time as follows

$$\frac{d\tau}{dt} = \omega_E \frac{\eta^2}{\eta^2 - 1}, \tag{11}$$

(10) could be written in the form of Hamilton's canonical equations, i.e.,

$$\frac{d\eta}{d\tau} = -\frac{\partial H}{\partial \theta}, \quad \frac{d\theta}{d\tau} = \frac{\partial H}{\partial \eta}, \tag{12}$$

where

$$H = \log \frac{(1+\eta)^2}{\eta} - \frac{\gamma}{\omega_E}\left(\eta - \frac{1}{\eta}\right)\sin 2(\theta - \alpha) + \frac{1}{2}\frac{\omega_R}{\omega_E}\frac{\eta^2 + 1}{\eta}. \tag{13}$$

Unfortunately, when we want to consider the situation where γ, α, ω_R vary in time this form of the equations poses severe difficulties since the "time τ" in (12) giving the time evolution of η and θ is not homogeneous in the physical time.

However, it is possible to transform the system into Hamiltonian form in such a way that this problem does not occur. We first non-dimensionalize the parameters by letting

$$(\eta, \alpha, \omega_R) \mapsto (\sigma, \alpha, \kappa) = \left(\frac{\gamma}{\omega_E}, \alpha, \frac{\omega_R}{\omega_E}\right), \tag{14}$$

and then we let

$$(I, \varphi, \tau) = \left(\frac{(\eta - 1)^2}{\eta}, 2\theta, 2\omega_E t\right). \tag{15}$$

I corresponds to the self-induced angular momentum of the UEV in the absence of the external linear flow field, and φ represents the inclination of the UEV in a way that does not distinguish the fact that the UEV configuration is unchanged by a 180° increase of θ. In these coordinates the equations take the following form

$$\begin{pmatrix} \frac{dI}{d\tau} \\ \frac{d\varphi}{d\tau} \end{pmatrix} = \begin{pmatrix} \sigma\sqrt{I^2 + 4I}\cos\left(\varphi - \frac{\alpha}{2}\right) \\ \frac{1}{I+4} - \sigma\frac{I+2}{\sqrt{I^2+4I}}\sin\left(\varphi - \frac{\alpha}{2}\right) + \frac{\kappa}{2} \end{pmatrix} = \begin{pmatrix} -\frac{\partial H}{\partial \varphi} \\ \frac{\partial H}{\partial I} \end{pmatrix}, \tag{16}$$

where

$$H(I, \varphi; \sigma, \alpha, \kappa) = H_E(I) + H_S(I, \varphi; \sigma, \alpha) + H_R(I; \kappa), \quad H_E(I) = \log(I + 4),$$

$$H_S(I, \varphi; \sigma, \alpha) = -\sigma\sqrt{I^2 + 4I}\sin(\varphi - \alpha/2), \quad H_R(I; \kappa) = \frac{\kappa}{2} I. \tag{17}$$

The Hamiltonian H can be interpreted physically as the total excess kinetic energy of the flow field with H_E, H_S, and H_R being the contributions from the UEV, linear external strain, and linear external rotation, respectively. This decomposition will be useful in that it will allow us to give a description of the UEV motion in terms of "energetics".

In some cases the analysis of (16) is more straightforward if we use another set of canonical variables, (δ, ζ), which are the cartesian coordinates of the polar coordinates defined as follows:

$$(\delta, \zeta, \tau) = (\sqrt{2I}\cos\varphi, \sqrt{2I}\sin\varphi, \tau). \tag{18}$$

This coordinate transformation also has the advantage of eliminating the singularity at $I = 0$. Accordingly, the equations of motion in these variables have the form

$$\begin{pmatrix} \dfrac{d\delta}{d\tau} \\ \dfrac{d\zeta}{d\tau} \end{pmatrix} = \begin{pmatrix} \dfrac{-2\zeta}{\delta^2+\zeta^2+8} + \dfrac{\sigma}{2}\dfrac{(\delta^2+2\zeta^2+8)\cos(\alpha/2) - \delta\zeta\sin(\alpha/2)}{\sqrt{\delta^2+\zeta^2+8}} - \dfrac{\kappa}{2}\zeta \\ \dfrac{2\delta}{\delta^2+\zeta^2+8} - \dfrac{\sigma}{2}\dfrac{\delta\zeta\cos(\alpha/2) - (2\delta^2+\zeta^2+8)\sin(\alpha/2)}{\sqrt{\delta^2+\zeta^2+8}} + \dfrac{\kappa}{2}\delta \end{pmatrix} = \begin{pmatrix} -\dfrac{\partial H}{\partial \zeta} \\ \dfrac{\partial H}{\partial \delta} \end{pmatrix}, \tag{19}$$

with the Hamiltonian function given by

$$H(\delta, \zeta; \sigma, \alpha, \kappa) = H_E(\delta, \zeta) + H_S(\delta, \zeta; \sigma, \alpha) + H_R(\delta, \zeta; \kappa), \quad H_E(\delta, \zeta) = \log\left(\frac{\delta^2+\zeta^2+8}{2}\right),$$

$$H_S(\delta, \zeta; \sigma, \alpha) = -\frac{\sigma}{2}\sqrt{\delta^2+\zeta^2+8}\left(\zeta\cos\frac{\alpha}{2} - \delta\sin\frac{\alpha}{2}\right), \quad H_R(\delta, \zeta; \kappa) = \frac{\kappa}{4}(\delta^2+\zeta^2). \tag{20}$$

3. UEV dynamics in time-independent linear velocity fields

In this section we describe the dynamics of the UEV when the parameters σ, α, and κ are constant in time. Without loss of generality we can take $\alpha = 0$ by choosing the Lagrangian frame axes to be aligned with the steady straining axis. The main reason for presenting this section on UEV dynamics in time-independent linear velocity fields is for completeness, as the focus of this work is on the situation of UEV's in unsteady linear velocity fields. The phase space structure in the steady case will form the basis for our analysis of the unsteady case as many of our arguments will be perturbative in nature where we consider time-dependent perturbations of steady linear velocity fields.

In particular, we are interested in all possible solutions to equations (19). These equations depend on the two parameters σ and κ, and as these parameters are varied we would expect bifurcations of solutions to occur. As mentioned earlier, both Kida (1981) and Neu (1984) have analyzed the steady case. However, our work on UEV's in unsteady linear external velocity fields requires us to extend their work in certain modest ways. In particular, Kida gives a bifurcation diagram in the $\kappa - \alpha$ plane (in his notation, the $2\gamma/\omega - e/\omega$ plane), however, he does not describe the different possible phase portraits. On the other hand, Neu gives phase portraits, however he does not consider the effects of an external linear vorticity field. In our terminology, this means he

takes $\kappa = 0$. Thus our work fills in certain gaps in this area and we go further in describing the different possible motions as an interchange of different parts of the total excess kinetic energy. This latter feature will illuminate our results in the unsteady case.

3.1. Dynamics and bifurcations

In this section, we present all the possible solutions of (19) in the $\delta - \zeta$ phase space as a function of the parameters (κ, σ). Because the system is autonomous and Hamiltonian, the solution curves in the $\delta - \zeta$ phase space are given by the level curves of the Hamiltonian function (H). We begin by discussing the typical orbits in the $\delta - \zeta$ phase space, and then consider the solution structure and bifurcations in relation to the parameter values.

We show that the possible motions, for any parameter values, are one of the following:

(i) fixed points,
(ii) periodic orbits,
(iii) homoclinic orbits,
(iv) orbits connecting a hyperbolic fixed point to infinity,
(v) unbounded orbits.

Now we describe the solution structure in the $\delta - \zeta$ phase space corresponding to different parameter values (κ, σ). The bifurcation diagram is given in Fig. 3.

The curves $S^{\pm}, G^{\pm}, I_1^{\pm}, I_2^{\pm}, U^{\pm}$ and R in Fig. 3 are called bifurcation curves and define the boundaries of the regions in the (κ, σ) plane corresponding to topologically distinct UEV motions. We will not derive explicit formulae for these curves here, the reader should consult Kida [1981] or Ide [1990]. Note that the bifurcations on $G^{\pm}$ and $U^{\pm}$ are associated with the singularities at $I = 0$ in (16) and they are not bifurcations in the $\delta - \zeta$ phase space in the sense usually discussed. However, since the UEV motion exhibits qualitatively different dynamics upon crossing these curves, we treat them as bifurcations.

In Fig. 4 we show the "metamorphoses" of phase portraits corresponding to the numbers in Fig. 3 that occur upon crossing the bifurcation curves.

We now give a brief description of the dynamics near the bifurcation curves $S^+, G^+, I_1^+, I_2^+, U^+$ and R. The dynamics near S^-, G^-, I_1^- and I_2^- are easily obtained by noting that Eqs. (19) are unchanged under the change of variables $(\delta, \zeta, \sigma, \kappa) \to (-\delta, -\zeta, -\sigma, \kappa)$. Thus the phase portraits corresponding to the point $(\kappa, -\sigma)$ correspond to the phase portrait at the point (κ, σ), *but rotated* 180°.

S^+: *Hamiltonian Saddle-node bifurcation.* This is a standard bifurcation.

G^+: *Global bifurcation at the origin.* As we pass G^+ from above to below the homoclinic orbit crosses the δ-axis and encircles the origin of the $\delta - \zeta$ phase space as shown in Fig. 4. This has important dynamical consequences for the UEV motion that we will discuss in the next section.

I_1^+: *Bifurcation at infinity on the positive ζ-axis.* The hyperbolic fixed point moves to infinity and disappears.

U^+: *Bifurcation at the origin for the elliptic fixed point.* As we cross U^+ from above to below the elliptic fixed point moves from the positive ζ-axis to the negative ζ-axis. We will discuss the dynamical consequences of this in the next section.

I_2^+: *Bifurcation at infinity on the negative ζ-axis.* As we cross I_2^+ from above to below an elliptic fixed point is born at infinity on the negative ζ-axis.

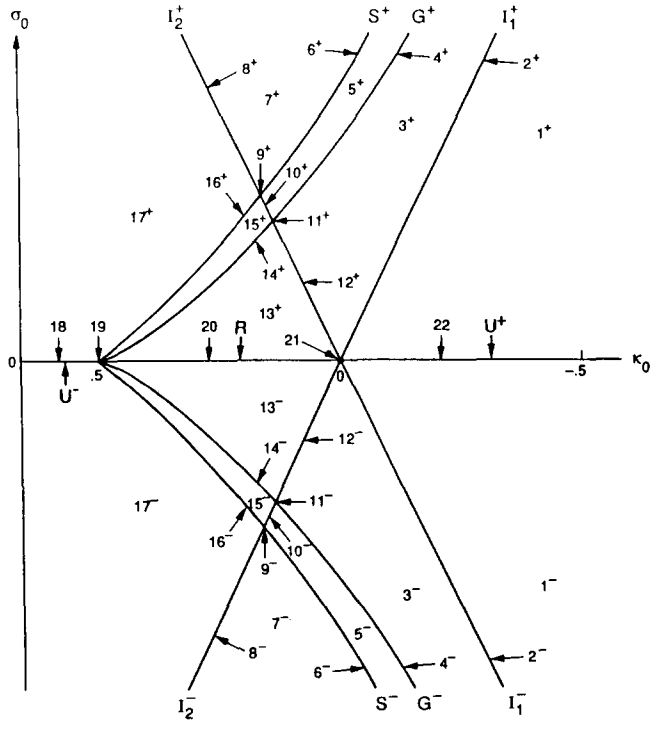

Fig. 3. The bifurcation diagram.

S^+: *below* I_2^+: *Saddle-node bifurcation on a periodic orbit.*

U^-: *Bifurcation at the origin for an elliptic fixed point.*

R: *Ring bifurcation.* As we approach R from above, an elliptic fixed point moves toward the origin while both the inner homoclinic orbit (IHO) and the outer homoclinic orbit (OHO) coalesce and turn into a circle of fixed points inside which the elliptic fixed point disappears as shown in Fig. 4.

3.1.1. Interpretation of phase space dynamics and bifurcations in terms of the motion in physical space

Having described the solution of (19) in the $\delta - \zeta$ phase space as a function of the parameter (κ, σ), we now interpret these solutions in terms of the UEV motion.

The bifurcation analysis was most easily performed in the $\delta - \zeta$ coordinate system. However, for describing the motion of the UEV in physical space it will often be more clear to return to either the (η, θ) coordinates or the (I, φ) coordinates. Recall from the discussion of the different coordinate systems in the previous section that $\theta = \varphi/2$, $\eta = a/b$, and $I = (\eta - 1)^2/\eta$ with $(\delta, \zeta) = (\sqrt{2I}\cos\varphi, \sqrt{2I}\sin\varphi)$. We make the important remark that all rescalings of time were by constant factors. This will be significant when we consider time dependent external velocity fields. Since the UEV dynamics can be understood as the change of UEV configuration (η, θ) and/or motion of a point at the tip of UEV semi-major axis $(\sqrt{\eta}, \theta)$, we first define the terminology for two main features of

UEV dynamics in terms of the rate of change in (I, φ). We call $dI/d\tau$ the deformation rate of the vortex shape and note that $dI/d\tau > 0$ implies $d\eta/d\tau > 0$ which corresponds to elongation of a UEV. Similarly, $dI/d\tau < 0$ implies $d\eta/d\tau < 0$ which corresponds to contraction of a UEV. Additionally, we refer to $d\varphi/d\tau$ as the modified angular velocity of the semi-major axis. In general, we can have $d\varphi/d\tau > 0$ or $d\varphi/d\tau < 0$ corresponding to counterclockwise (c-c) motion or clockwise (c) motion, respectively.

We next describe the five typical orbits described in the previous section in terms of UEV motion.

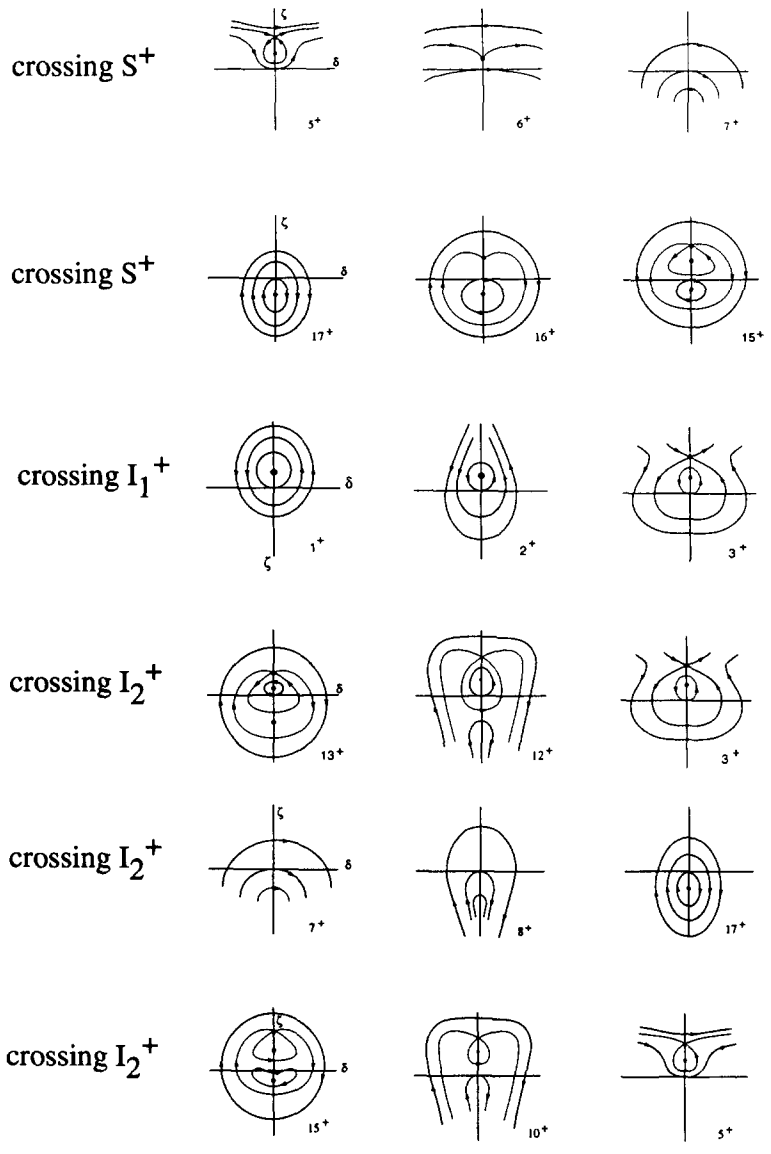

Fig. 4. (Continued).

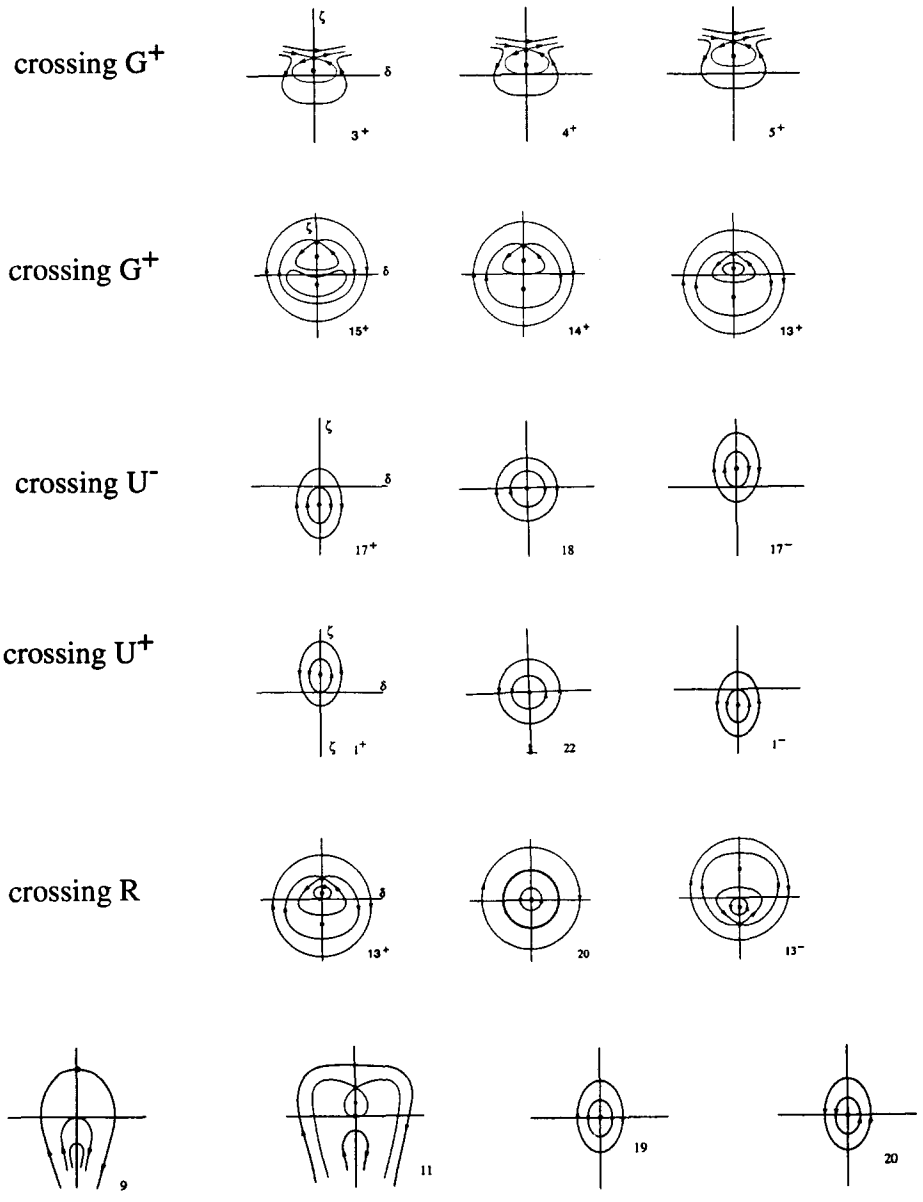

Fig. 4. Phase portraits in the different regions of the bifurcation diagram. Phase portraits labelled 9, 11, 19, and 21 lie on the intersection of two bifurcation curves and are, thus, combinations of those particular two bifurcations. 19 corresponds to the birth of a fixed point at the origin that immediately expands into a circle of fixed points (as parameters are varied). 20 corresponds to this circle of fixed points disappearing at ∞.

(i) A fixed point corresponds to a steady UEV which does not change its configuration (η, θ) for all time. A hyperbolic fixed point (an elliptic fixed point, resp.) corresponds to an unstable (stable, resp.) steady UEV. Any UEV whose initial configuration (IC) is slightly shifted from a stable steady UEV configuration undergoes a periodic oscillatory motion with small change in its configuration,

which corresponds to a periodic orbit around the elliptic fixed point, as we will see in (2). This may not be the case for a UEV whose IC is slightly perturbed from an unstable steady UEV configuration. Since all the fixed points in the $\delta - \zeta$ phase space exist only on the ζ-axis, a UEV can be steady only at special inclination angles that are easily computed and found to be $\theta(= \varphi/2) = \pi/4$ and $\theta(= \varphi/4) = 3\pi/4$.

(ii) The periodic motions of the UEV can be classified into six distinct types depending on (1) the direction of motion and (2) whether or not the periodic orbit contains the origin (in the $\delta - \zeta$ plane) in its interior. If the origin is *not* contained inside the interior of the periodic orbit then the angle φ cannot exceed 2π. This periodic motion is referred to as *oscillation*. If the origin *is* contained in the interior of the periodic orbit, then φ can increase or decrease through 2π, and the resulting periodic motion is referred to as *rotation*. In the case of a periodic orbit passing through the origin, the angle φ becomes undefined at the origin. This critical periodic orbit is special in that it separates oscillation from rotation. We refer to it as a periodic boundary orbit (PBO).

Hence the six types of periodic motions are:

(a) Oscillation about $\theta(= \varphi/2) = \pi/4$. In this case the tip of the semi-major axis of the UEV moves along a closed curve in a counter-clockwise sense.
(b) Rotation in a counterclockwise sense.
(c) Counterclockwise periodic orbit passing through the origin.
(d) Oscillation about $\theta(= \varphi/2) = 3\pi/4$. In this case the top of the semi-major axis of the UEV moves along a closed curve in a clockwise sense.
(e) Rotation in a clockwise sense.
(f) Clockwise periodic orbit passing through origin.

(iii) A homoclinic orbit corresponds to a UEV motion which asymptotically approaches an unstable steady state in positive and negative time. The motion is said to be rotational or oscillatory depending on whether or not the orbit encloses the origin of the $\delta - \zeta$ phase space. Furthermore, homoclinic orbits define boundaries separating regions of qualitatively distinct UEV motions. If IHO (inner homoclinic orbit) is the only homoclinic orbit in the $\delta - \zeta$ phase space, then it divides the $\delta - \zeta$ plane into an interior region corresponding to a (c-c) periodic motion and an exterior region corresponding to irreversible elongation which we discuss next. When both IHO and OHO (outer homoclinic orbit) exist in the $\delta - \zeta$ phase space, for some values of (κ, σ), they define the boundaries of three regions: the interior of IHO ((c-c) periodic motion), the region bounded by IHO and OHO ((c) periodic motion and the exterior of OHO ((c) periodic motion).

(iv) The orbits connecting the hyperbolic fixed point to infinity, i.e., the branches of the stable and unstable manifolds of the hyperbolic fixed point that do not belong to a homoclinic orbit, correspond to irreversible contraction of the UEV (on the stable manifold) along the contraction axis θ_c and irreversible elongation of the UEV (on the unstable manifold) along the elongation axis θ_e where

$$\theta_c = \pi/2 - \sin^{-1}(\kappa/2\sigma), \qquad \theta_e = \sin^{-1}(\kappa/2\sigma).$$

(v) Unbounded orbits correspond to irreversible elongation of the UEV along axes fixed at the angles θ_c and θ_e. These orbits are classified into two types depending on the direction of elongating

motion, i.e., (c-c) elongation and (c) elongation. The boundaries of these two regions are defined by certain orbits described as follows.

Case 1: The origin of the $\delta - \zeta$ phase space is not enclosed by a homoclinic orbit. An unbounded orbit which goes through the origin defines the boundary as shown in Fig. 4.

Case 2: The origin of the $\delta - \zeta$ phase space is enclosed by a homoclinic orbit. The branches of the stable and unstable manifold of the hyperbolic fixed point that go to infinity define the boundary.

The orbits which define the boundary are called unbounded boundary orbits (UBO's). The unbounded orbits above UBO's in the $\delta - \zeta$ phase space correspond to (c) irreversible elongation and the unbounded orbits below UBO's corresponds to (c-c) elongation.

3.2. The motion of an UEV in physical space and its description in terms of the excess kinetic energy decomposition

The UEV motion for a given initial configuration (I_0, φ_0) and an external linear flow field $(\sigma, \alpha, \kappa) = (\sigma_0, \alpha_0 = 0, \kappa_0)$ conserves the total excess kinetic energy H of the entire flow domain. In this section, we discuss the decomposition of H into H_E, H_S and H_R as described in the first section and describe how the external flow parameters (κ, σ) influences the UEV dynamics in terms of these three components of kinetic energy. Fig. 5 shows the level curves of H_E, H_S and H_R in the $\delta - \zeta$ phase space.

Because the time variable τ is normalized by the UEV vorticity ω_E, the sign of the Hamiltonian functions H_S and H_R corresponds to the direction of the motion induced by each effect. For example, if $H_S > 0$, then the corresponding motion induced by the straining effect is in the same direction as the self-induced motion, i.e., $\mathrm{d}\varphi/\mathrm{d}r|_S > 0$. Similarly, $H_S > 0$, then the corresponds to $\mathrm{d}\varphi/\mathrm{d}\tau|_S < 0$. Note that every level curve of H_E is circular, and H_E has its minimum at the origin $(I = 0)$ with $H_E(0) = \log 4$. This results in all periodic motion being (c-c) rotations when $\kappa_0 = \sigma_0 = 0$. In Fig. 5, which shows that the level curves of H_S, $\varphi = 0$ and $\varphi = \pi$ correspond to contracting and stretching axes of the straining field, respectively. H_S is negative for $0 < \varphi < \pi$ because the flow field induced by the straining effect acts against the self-induced motion (i.e., the induced flow field is in clockwise direction). H_S is positive for $\pi < \varphi < 2\pi$ because the induced flow field is in the same direction as the self-induced motion. The straining effect is most effective on $\varphi = \pi/2, \frac{3}{2}\pi$ (i.e., a level curve of H_S is tangent to a level curve of H_R on those axes).

Any level curve of H_S is circular as is shown in Fig. 5. If $\kappa_0 > 0$ (i.e., $H_S > 0$), then the flow field induced by the background vorticity is in the same direction as the self-induced motion. H_S has one minimum at $I = 0$, and all the corresponding motions are (c-c). Similarly for $\kappa_0 < 0$, H_R is negative with one maximum at $I = 0$, and all the corresponding motions are (c).

The asymptotic behavior of H_E, H_S and H_R for $I \ll 1$ and $I \gg 1$ can easily be deduced from (17) and is as follows

$$H_E \sim \begin{cases} \log 4 + \frac{1}{4}I, & I \ll 1, \\ \log I, & I \gg 1, \end{cases} \tag{21}$$

$$H_S \sim \begin{cases} -2\sigma_0\sqrt{I}\sin\varphi, & I \ll 1, \\ -\sigma_0 I \sin\varphi, & I \gg 1, \end{cases} \tag{22}$$

$$H_R = \frac{\kappa_0}{2} I. \tag{23}$$

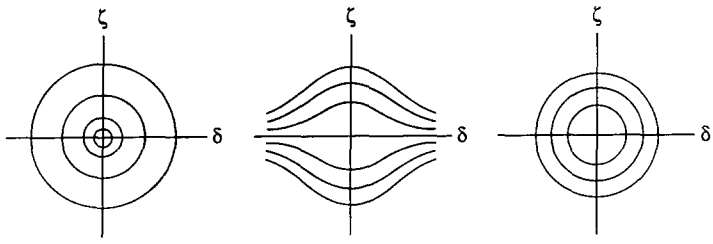

Fig. 5. Level curves of H_E, H_S, and H_R in the $\delta - \zeta$ phase space.

For $I \gg 1$ the UEV dynamics (i.e., vortex sheet dynamics) is dominated by the external flow field. Let us first consider the mechanism for irreversible elongation. Irreversible elongation occurs when H_S dominates H_R for $I \gg 1$. This is possible only for $\sigma_0 \geqslant |\kappa_0|/2$. Another way of understanding irreversible elongation is as follows. On the elongation axis for $I \gg 1$, a UEV deforms without change in φ i.e., change in I does not affect H although change in φ does affect H since $\partial H/\partial I = 0$ and $\partial H/\partial \varphi \neq 0$ on the elongation axis. Note that if H_R dominates H_S for $I \gg 1$ (i.e., $|\kappa_0|/ \geqslant \sigma_0$), then the UEV undergoes periodic rotation with a large aspect ratio.

We only mention here that the bifurcations occurring on $S^{\pm}$, $I^{\pm}_{1,2}$, $U^{\pm}$ and R can be explained in terms of the balance of excess kinetic energy. A complete discussion of this can be found in Ide (1990).

We now give a qualitative discussion concerning how the three components of the excess kinetic energy interchange during the evolution, while conserving the total excess kinetic energy, for a given external flow field (κ_0, σ_0). From (17), we have

$$\frac{\mathrm{d}}{\mathrm{d}\tau} H = 0 = \frac{\mathrm{d}}{\mathrm{d}\tau} H_E + \frac{\mathrm{d}}{\mathrm{d}\tau} H_S + \frac{\mathrm{d}}{\mathrm{d}\tau} H_R, \tag{24}$$

where each of the rate of change in kinetic energies is evaluated on an orbit defined by a constant H curve. Since every orbit is symmetric around $\varphi = \pi/2$ and $\frac{3}{2}\pi$ for any parameter (κ_0, σ_0), we only need to consider the case $-\pi/2 < \varphi < \pi/2$. The qualitative behavior of each component of kinetic energy along the different types of orbits are described as follows;

$(\mathrm{d}/\mathrm{d}\tau) H_E$

$$\frac{\mathrm{d}}{\mathrm{d}\tau} H_E \begin{cases} > 0 & \text{on IHO,} \\ < 0 & \text{on OHO} \\ > 0 & \text{on (c-c) periodic orbit,} \\ < 0 & \text{on (c) periodic orbit.} \end{cases} \tag{25}$$

$(\mathrm{d}/\mathrm{d}\tau)H_R$

$$\frac{\mathrm{d}}{\mathrm{d}\tau}H_R \begin{cases} > 0 & \text{on IHO for } \kappa_0 > 0, \\ < 0 & \text{on IHO for } \kappa_0 < 0 \\ < 0 & \text{on OHO} \\ > 0 & \text{on(c-c) orbit for } \kappa_0 > 0, \\ < 0 & \text{on (c-c) orbit for } \kappa_0 < 0, \\ < 0 & \text{on (c) periodic motion.} \end{cases} \tag{26}$$

$(\mathrm{d}/\mathrm{d}\tau)H_S$

$$\frac{\mathrm{d}}{\mathrm{d}\tau}H_S \begin{cases} < 0 & \text{on IHO,} \\ < 0 & \text{on (c-c) orbit} \\ > 0 & \text{on OHO for } I < I_0 \\ < 0 & \text{on OHO for } I > I_0 \\ > 0 & \text{on (c) orbit for } I < I_0 \\ < 0 & \text{on (c) orbit for } I > I_0. \end{cases} \tag{27}$$

with

$$I_0 = \begin{cases} -(4 + 2/\kappa_0), & \text{if } \kappa_0 < -\tfrac{1}{2}, \\ 0, & \text{otherwise.} \end{cases} \tag{28}$$

A detailed discussion can be found Ide (1990).

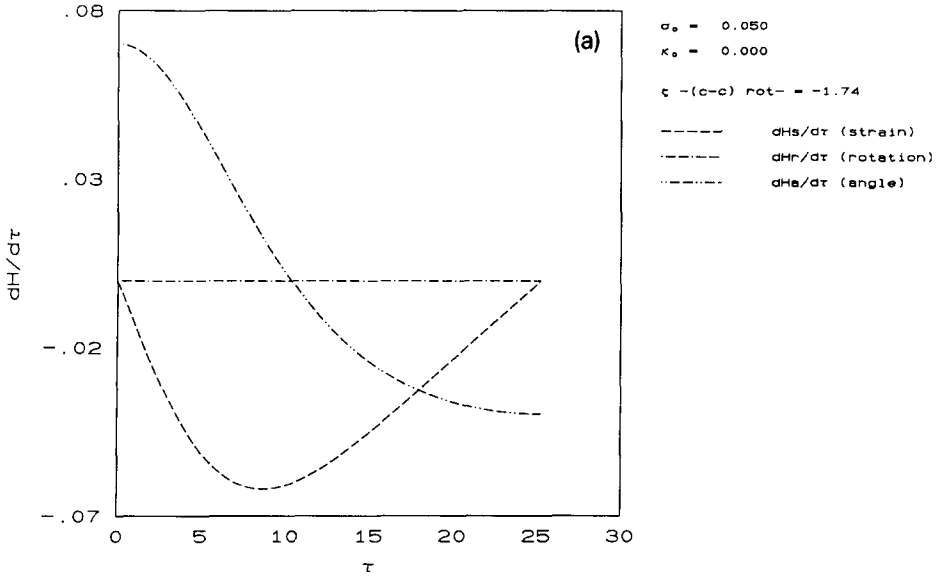

Fig. 6. Plots of $(\mathrm{d}/\mathrm{d}\tau)H_E$, $(\mathrm{d}/\mathrm{d}\tau)H_S$ and $(\mathrm{d}/\mathrm{d}\tau)H_R$ for three different type of unperturbed orbits. All integrations are started on the ζ axis at the points indicated in the respective figures. (a) $(\sigma_0, \kappa_0) = (0.05, 0)$, (b) $(\sigma_0, \kappa_0) = (0.05, 0)$, (c) $(\sigma_0, \kappa_0) = (0.05, -0.15)$.

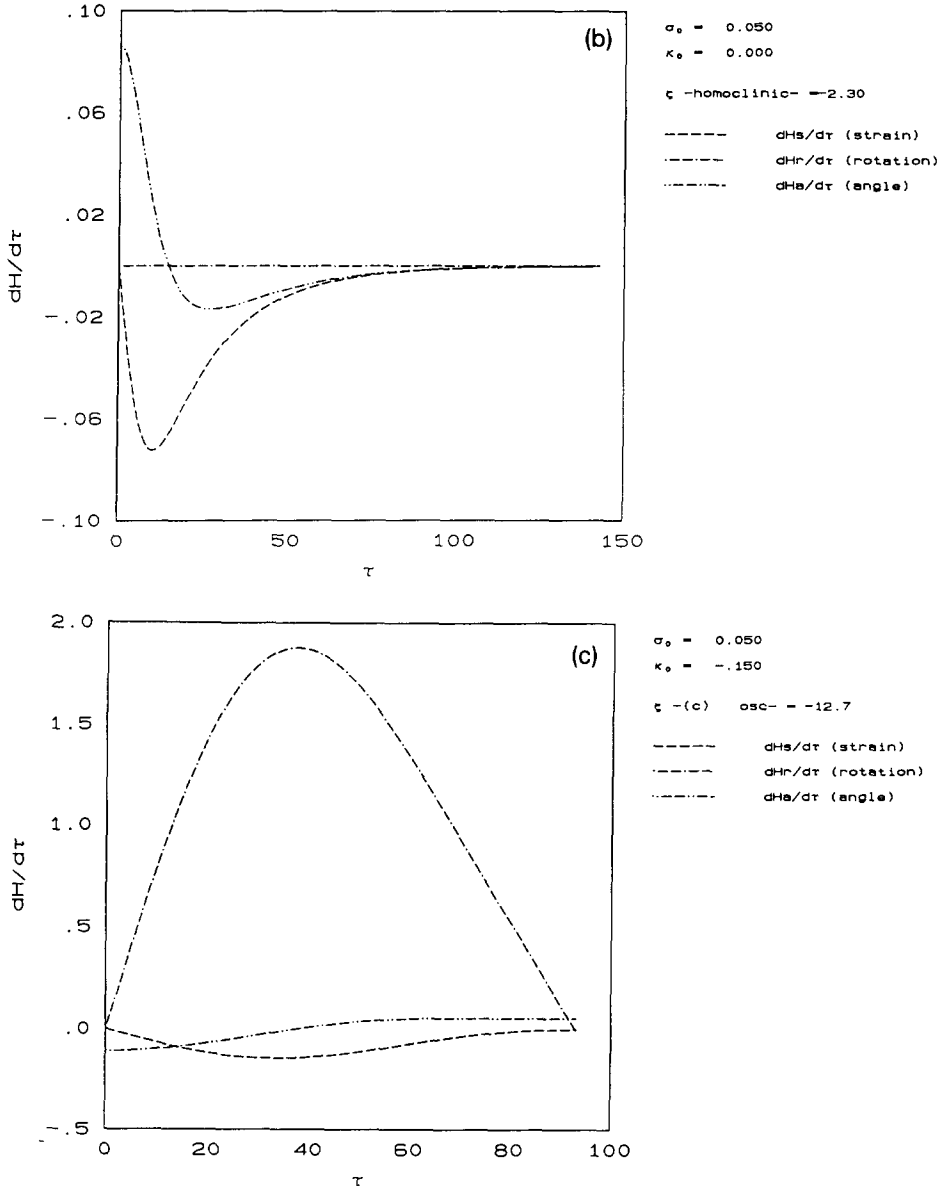

Fig. 6. (Continued).

We note from (21)–(23) that $(d/d\tau)H_E$ dominates $(d/d\tau)H_R$ for $I < I_0$ and $(d/d\tau)H_R$ dominates $(d/d\tau)H_E$ for $I < I_0$. $(d/d\tau)H_S$ balances the difference of $(d/d\eta)H_E$ and $(d/d\eta)H_R$. Some typical behaviors of $(d/d\eta)H_E, (d/d\tau)H_S$ and $(d/d\eta)H_R$ are shown in Figs. 6a, b for parameter values, $(\sigma_0, \kappa_0) = (0.05, 0)$ corresponding to region 3^+ in Fig. 3. This phase portrait corresponding to these parameter values contains (c-c) periodic orbits (corresponding to oscillation and rotation), and

an inner homoclinic orbit. Fig. 6c is for $(\sigma_0, \kappa_0) = (0.05, -0.15)$ corresponding to region 13^+ in Fig. 3. The corresponding phase portrait includes (c) periodic orbits.

We will see later when we introduce the Melnikov technique that the rate of change in H_S and H_R are important for understanding the UEV dynamics in unsteady external flow fields.

4. UEV dynamics in time-periodic linear velocity fields

We will now consider the dynamics of UEV's in time-periodic, linear velocity fields. In particular, we let

$$\sigma(\tau) = \sigma_0[1 + \varepsilon_\sigma \sin \Omega(\tau + \tau_\sigma)], \quad \alpha(\tau) = \varepsilon_\alpha \sin \Omega(\tau + \tau_\alpha),$$

$$\kappa(\tau) = \kappa_0[1 + \varepsilon_\kappa \sin \Omega(\tau + \tau_\kappa)]. \tag{29}$$

where $\varepsilon_\sigma, \varepsilon_\alpha, \varepsilon_\kappa$ are perturbation amplitudes with ε representing small perturbation parameter, and $\tau_\sigma, \tau_\alpha, \tau_\kappa$ are phase shifts for each perturbation type. The equations of motion will take the form of a time-periodically perturbed, one and a half-degree-of-freedom Hamiltonian system. Such systems have received intensive study in the dynamical systems community over the past 15 years and therefore a variety of techniques are at our disposal. In particular, since the equations are time periodic with period $2\pi/\Omega$, we will study the dynamics by studying the associated *Poincaré map*, i.e., the two-dimensional area-preserving transformation $(I(0), \phi(0)) \mapsto (I(2\pi/\Omega), \phi(2\pi/\Omega))$ or $(\delta(0), \zeta(0)) \mapsto (\delta(2\pi/\Omega), \zeta(2\pi/\Omega))$. *It is important to note that σ_0 and κ_0 are not allowed to lie on the bifurcation curves I_1^+, I_2^+, S^+ and R in Fig.* 3. In such cases the standard Melnikov method would not apply immediately.

We begin by considering certain solutions of (19) in the steady case, i.e., where σ, κ, and α are constant, and discussing what becomes of them under the time-periodic perturbation.

Fixed Points: It is a standard result that for sufficiently small Hamiltonian perturbations, elliptic fixed points and hyperbolic fixed points remain as fixed points in the perturbed Poincaré map without changing their stability type. In the continuous time system, these are periodic orbits of the same stability type with period $2\pi/\Omega$. These small amplitude periodic UEV motions generated from the fixed points in the unperturbed flow are usually small oscillation, and very rarely rotation, except when the perturbed periodic orbit encloses the origin of $\delta - \zeta$ coordinate system (which may occur for parameter sets near 18^+, 19^+, 20^+, 21^+ and 22^+ in Fig. 3)

Periodic Orbits: Let $T^H = 2\pi/\Omega^H$ denote the period of an *unperturbed* periodic orbit. For the unperturbed Poincaré map this periodic orbit is manifested as an *invariant circle*. We define the *rotation number*, denoted ρ, of this invariant circle as

$$\rho = T^H/T, \tag{30}$$

where $T \equiv 2\pi/\Omega$ is the period of the perturbation. For the perturbed Poincaré map, there are two types of dynamics depending on ρ:

$\rho = m/n =$ rational, where m and n are relatively prime integers: In this case, during m iterates of the unperturbed Poincaré map, every orbit on the invariant circle makes n complete revolutions along the circle and returns to its original position. Under the perturbation, this invariant circle will

generically break up into a *resonance band*. The subharmonic Melnikov method (Wiggins, 1990) will be applied to study this situation.

ρ = irrational: In this case, any orbit on the invariant circle never returns to its original position, i.e., the orbit densely fills out the circle. Under the perturbation the invariant circle will typically be preserved as a KAM torus or possibly a cantorus, provided the twist condition is satisfied. These are quasiperiodic motions that fill out a circle and Cantor set, respectively, see Wiggins (1992). The UEV motion on a KAM torus is much the same as the similar unperturbed motions in the steady linear external velocity fields.

Homoclinic and Heteroclinic Orbits: These will generically break up to form transversal homoclinic and heteroclinic orbits. Associated with transversal homoclinic orbits are chaotic dynamics in the sense of 5 male horseshoes. If the transversal heteroclinic orbits actually form a heteroclinic cycle, as they do on a resonance band, then Smale horseshoes may also be constructed. Melnikov's method can be used to study this situation. Nearby unbounded orbits may also be created, such orbits may correspond to bounded orbits in the absence of time dependence.

Unbounded Orbits: The behavior along these orbits is qualitatively the same for the unperturbed and perturbed systems.

In the following, we consider UEV dynamics whose corresponding original unperturbed orbits are periodic and homoclinic orbits. In Sections 4.1 and 4.2 we give qualitative discussion of the solution of perturbed system and corresponding UEV motion, which is followed in Sections 4.3 and 4.4 by a description of the analytical results that allow us to prove these assertions as well as a discussion of the physical implications using the Melnikov methods.

4.1. UEV dynamics associated with resonance bands

4.1.1. The creation of resonance bands and typical UEV dynamics

When the time periodic perturbation is imposed on a periodic orbit, the unperturbed invariant circle with resonance relation $m\Omega^{\mathrm{H}} = n\Omega$ may break up into $2ml$ period m points where l is some integer that may depend on the geometry of the unperturbed orbit and the perturbation functions (Ide, 1990). Generically, of the $2ml$ period m points, ml are hyperbolic period m points and ml are elliptic period m points that are ε-close to the unperturbed invariant circle and alternate in stability type as one traverses the invariant circle. The stable and unstable invariant manifolds of the hyperbolic period m points generically intersect transversely and form heteroclinic tangles that surround the neighboring elliptic period m points. This results in a chain-like structure, the so-called resonance band of order m/n (henceforth referred to as "RB m/n").

The existence of RB m/n is proven for $n = 1$ using $\mathcal{O}(\varepsilon)$ Melnikov methods in Section 4.3 and 4.4. $2ml$ period m points of RB $m/1$ represent periodic UEV motion with period $2\pi m/\Omega$ in the continuous time system. If the orbit corresponding to the UEV motion is contained in RB $m/1$, then the UEV typically oscillates (or rotates) with a fairly large fluctuation amplitude from its original unperturbed motion. The UEV motion can also be chaotic if the corresponding orbit lies in the chaotic Cantor set associated with the heteroclinic tangles of RB $m/1$. In Fig. 7 we give an illustration of the resonance bands and associated heteroclinic tangles for the Poincaré map.

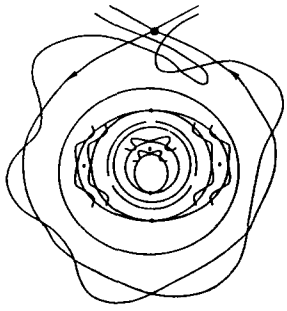

Fig. 7. Resonance bands and associated heteroclinic tangles for the Poincaré map.

4.1.2. Transition dynamics due to RB m/1 along PBO

Recall that, in a steady external linear flow field, the boundary orbits (i.e., PBO, IHO and OHO) in the phase space divide two regions corresponding to qualitatively different types of UEV motion, where PBO is a periodic orbit going through the origin of the (δ, ζ) coordinate system ((c-c) PBO for (κ_0, σ_0) in $1^+, 3^+, 13^+$ and (c) PBO for 15^+, 17^+). In unsteady external flow fields, these boundary orbits may break up and enable an important phenomenon, i.e., *transition dynamics* where the UEV exhibits more than one types of motion during its evolution, to occur. There are two mechanisms which cause the transition dynamics; one is RB m/n along PBO and the other is homoclinic tangles along IHO and OHO. The transition dynamics along the PBO can occur when the origin lies in a RB m/n. Then the orbit may fluctuate in the band with large amplitude which represents irregular motion of the UEV flipping its type of motion between oscillation and rotation. However, if the origin lies in KAM torus or cantorus, then the UEV motion is regular and there exists no transition dynamics between oscillation and rotation.

4.2. UEV dynamics along homoclinic tangles and heteroclinic cycles: chaos and transition dynamics

As a result of the break-up of homoclinic orbits (homoclinic tangles in Poincaré map), two new important dynamics now become possible; one is associated with Chaotic cantor sets and the other is the due to the so called "turnstile mechanism" associated with the tangles (see Wiggins, 1992). A discussion of the analytical methods for proving the existence of the transversal homoclinic orbits for each type of perturbation is left to Sections 4.3 and 4.4. In the regions denoted 3^+, 4^+ and 5^+ in Fig. 3 where there is only one homoclinic orbit in the phase space, there exists chaotic Cantor sets associated with the IHO tangle. In the regions denoted 13^+, 14^+ and 15^+ both IHO and OHO co-exist and intersect. In this situation there are chaotic Cantor sets associated with IHO, OHO, and with the intersection of the tangles associated with IHO and OHO.

Following Rom-Kedar *et al.* (1990), we may define a new "boundary" associated with each homoclinic tangle using segments of unstable and stable manifolds of hyperbolic fixed points in the

Poincaré map. Then the new boundaries re-define the regions corresponding to two qualitatively different types of UEV motion. We first examine the dynamics associated with the chaotic Cantor sets. In $3^+, 4^+$ and 5^+ of Fig. 3, the chaotic Cantor set associated with the IHO lies inside the new boundary. The corresponding UEV motion is hence chaotic (c-c) rotation for 3^+, chaotic (c-c) oscillation for 5^+, and chaotic (c-c) rotation and/or (c-c) oscillation near 4^+ depending on the position of the IHO tangle relative to the origin of the $\delta - \zeta$ coordinate system. In $3^+, 14^+$ and 15^+, the chaotic dynamics can be more complicated. The chaotic Cantor set associated with IHO lies inside the new boundary defined by the IHO tangle and leads to the same type of chaotic UEV motion as $3^+, 4^+$ and 5^+ respectively. The chaotic Cantor set associated with the OHO lies outside the new boundary defined by the OHO tangle and leads to chaotic (c) rotation for parameter values in the regions denoted 13^+, 14^+ and 15^+. Dynamics associated with chaotic Cantor sets which arise from the intersection of tangles associated with both IHO and OHO exhibits not only chaotic motion but also "transition dynamics" which we now discuss.

Together with chaotic motion, the transition dynamics along the tangles is an important phenomenon that arises only when the external linear velocity field is time-dependent. An orbit initially lying inside the new boundary may evolve across the boundary via the turnstile mechanism associated with the tangle, while another orbit initially outside the boundary may evolve inside of the boundary through the same mechanism. A complete discussion of this mechanism can be found in Wiggins (1992). What this implies for the UEV motion, in regions $3^+, 4^+$ and 5^+ of Fig. 3, is that a contracting UEV may become a (c-c) rotating (oscillating for 5^+, rotating and/or oscillating for 4^+) UEV, and possibly becoming an elongating UEV at a later time. Once a UEV change its dynamics to elongation, the motion is irreversible.

The dynamics in $13^+, 14^+$ and 15^+ due to the turnstile mechanism can be extremely complex as a result of the two intersecting tangles. In region 13^+, the UEV may change its type of motion repeatedly among (c-c) rotation, (c) oscillation and (c) rotation. Furthermore, transition dynamics can also be chaotic if the corresponding orbit belongs to 1^+ and 3^+. In 15^+, the motion may alternate among (c-c) oscillation, (c) oscillation and (c) rotation. In 14^+, the motion can include all types other than elongation, that is (c-c) oscillation, (c-c) rotation, (c) oscillation and (c) rotation. We illustrate these ideas in Fig. 8.

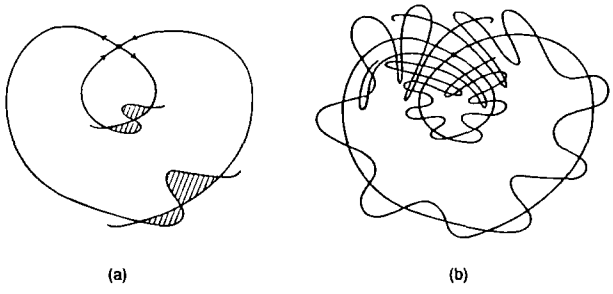

Fig. 8. (a) The turnstile mechanism for transition between regions corresponding to qualitatively different motions. (b) More of the homoclinic tangles.

4.3. *The subharmonic and homoclinic Melnikov methods*

So far our discussion have been mostly qualitative. In this section we recall the essential aspects of the subharmonic and homoclinic Melnikov methods that provide us not only with mathematical proofs for the above arguments but also insights into the underlying mechanisms of the resulting UEV motion related to each type of perturbation. Complete mathematical proofs as well as more details can be found in Wiggins (1990). The methods apply to time-periodic perturbations of one-degree-of-freedom Hamiltonian systems of the following form

$$\dot{x} = \frac{\partial H_0}{\partial y}(x, y) + \varepsilon \frac{\partial H_1}{\partial y}(x, y, t) + \mathcal{O}(\varepsilon^2), \tag{31}$$

$$\dot{y} = -\frac{\partial H_0}{\partial x}(x, y) - \varepsilon \frac{\partial H_1}{\partial x}(x, y, t) + \mathcal{O}(\varepsilon^2) \tag{32}$$

or, in a more convenient shorthand notation

$$\dot{q} = J\,\mathrm{D}H_0(q) + \varepsilon J\,\mathrm{D}H_1(q, t) + \mathcal{O}(\varepsilon^2), \tag{33}$$

where

$$J = \begin{pmatrix} 0 & 1 \\ -1 & 0 \end{pmatrix}, \tag{34}$$

and $q \equiv (x, y)$ with $D \equiv (\partial/\partial x, \partial/\partial y)$. The variable pair (x, y) represents either (I, φ) or (δ, ζ).

The subharmonic Melnikov theory is used to study the dynamics near RB m/n. Suppose for $\varepsilon = 0$ we have a one-parameter family of periodic orbits on which $(\partial/\partial H)T^H \neq 0$. Suppose we have a periodic orbit, $q^H(\tau)$, for which the following resonance relation holds

$$m\Omega^H = n\Omega. \tag{35}$$

We refer to this as a *resonant periodic orbit of order* m/n and henceforth denote such orbits as $q^{m/n}(\tau)$. The subharmonic Melnikov function, denoted $M^{m/n}(\tau_0)$, associated with this orbit is defined as follows:

$$M^{m/n}(\tau_0) = \int_{-mT/2}^{mT/2} \{H_0, H_1\}(q^{m/n}(\tau), \tau + \tau_0)\,\mathrm{d}\tau, \tag{36}$$

where $\tau_0 \in (-mT/2, mT/2]$ is a parametrization variable on the corresponding umperturbed orbit $q^{m/n}(\tau)$ and

$$\{H_0, H_1\} \equiv \frac{\partial H_0}{\partial x}\frac{\partial H_1}{\partial y} - \frac{\partial H_0}{\partial y}\frac{\partial H_1}{\partial x}$$

denotes the Poisson bracket of H_0 and H_1. Then the basic theorem of Melnikov tells us that the simple zeroes of $M^{m/n}(\tau_0)$, (i.e., $M^{m/n}(\tau_0) = 0$, $(\partial/\partial\tau_0)M^{m/n}(\tau_0) \neq 0$) correspond to the existence of period m points of RB m/n with alternating stability type between elliptic and hyperbolic.

Besides the existence of RB m/n, the Melnikov function $M^{m/n}(\tau_0)$ also gives us more information. It can be shown that $M^{m/n}(\tau_0)$ is related to the width of the RB m/n, denoted $d^{m/n}(\tau_0, \varepsilon)$. In

particular, $M^{m/n}(\tau_0)$ is the first order term of the width of the band, up to a known normalization factor, and is expressed as follows:

$$d^{m/n}(\tau_0, \varepsilon) = \varepsilon \frac{M^{m/n}(\tau_0)}{\| DH_0(q^{m/n}(-\tau_0)) \|} + O(\varepsilon^2). \tag{37}$$

It should be clear that $d^{m/n}$ is a measure of the fluctuation in the UEV configuration about the unperturbed motion.

We now want to consider the global structure of the Poincaré map associated with families of resonance bands. Suppose we have a family of unperturbed periodic orbits parametrized by $H \in (H_1, H_2)$, then the corresponding period T^H satisfies $T^H_{\min} < T^H < T^H_{\max}$ where $T^H_{\min} = \inf(T^{H_1}, T^{H_2})$, $T^H_{\max} = \sup(T^{H_1}, T^{H_2})$ and $(\partial/\partial H)T^H \neq 0$ for any $H \in (H_1, H_2)$. The corresponding natural frequency $\Omega^H = 2\pi/T^H$ ranges between $\Omega^H \in (\Omega^H_{\min}, \Omega^H_{\max}) = (2\pi/T^H_{\max}, 2\pi/T^H_{\min})$. If the family contains an elliptic fixed point q_e at its center, then $T^H_{\min} = T^{H(q_e)} = 2\pi/\Omega_e$ where Ω_e is the imaginary part of eigenvalues associated with the linearization of the vector field at q_e. Moreover, if the family is bounded by homoclinic orbits, then $T^H_{\max}$ goes to infinity logarithmically, in other words $\Omega^H_{\min}$ goes to zero, due to the presence of the hyperbolic fixed point q_h. The following results are easy to prove; more details can be found in the thesis of Ide (1990).

Perturbation frequency range for the existence of RB m/1.

We can compute the perturbation frequency range for which RB $m/1$ exists as follows. We let

$$\Omega^m_1 = m\Omega^H_{\min}, \qquad \Omega^m_2 = m\Omega^H_{\max}. \tag{38}$$

Then RB $m/1$ exists only if the perturbation frequency Ω satisfies the following condition.

$$\Omega \in (m\Omega^H_{\min}, m\Omega^H_{\max}). \tag{39}$$

The minimum frequency for the existence of RB m/1, of any order.

The minimum perturbation frequency that gives rise to a resonance band is $\Omega = \Omega^H_{\min}$ with the corresponding resonance band RB 1/1. For $\Omega < \Omega^H_{\min}$, there exists no RB $m/1$ for any m. This implies that low frequency perturbations do not excite order $m/1$ subharmonics. From this it follows that the UEV motion in unsteady external flow fields with low frequency is fairly regular for any initial configuration. As the frequency increases, the UEV motion near a stable steady configuration may begins to undergo oscillation.

The existence of a frequency gap of order k.

Suppose that there exists a k such that

$$\Omega^k_1 \equiv k\Omega^H_{\min}, \qquad \Omega^{k+1}_1 \equiv (k+1)\Omega^H_{\max}$$

where

$$\Omega^k_2 < \Omega^{k+1}_1. \tag{40}$$

Then, for all perturbation frequencies $\Omega \in (\Omega^k_2, \Omega^{k+1}_1)$, there exists n_0 unperturbed periodic orbits which satisfy the resonance relation $m\Omega^H = \Omega$, for any m. In other words, there exists no RB $m/1$ for any m for perturbation frequencies in this interval. We refer to this interval in the perturbation

frequency Ω (i.e., $\Omega \in (\Omega_2^k, \Omega_1^{k+1})$) as a *frequency gap of order k*. If the perturbation frequency of the external linear flow field for the UEV motion is in the frequency gap of order k, then the UEV motion is fairly regular for any initial configuration.

Frequency gap of order $k^* < k$.

Suppose that k satisfies the condition given in (40). Then there exists a frequency gap of order k^* for all $k^* < k$, and the frequency gap is given by $\Omega \in (\Omega_2^{k^*}, \Omega_2^{k^{*+1}})$.

Number of the frequency gaps N_g.

The number of the frequency gaps N_g and the highest order of a frequency gap are the same and are given by

$$N_g = \left(\frac{\Omega_{\min}^H}{\Omega_{\max}^H - \Omega_{\min}^H} + 1 \right). \tag{41}$$

The Melnikov method for transversal homoclinic points is similar to that for RB m/n. Suppose $q^{\text{homo}}(\tau)$ is a homoclinic orbit connecting a hyperbolic fixed point of the unperturbed system. Then the homoclinic Melnikov function is given by

$$M(\tau_0) = \int_{-\infty}^{+\infty} \{H_0, H_1\}(q^{\text{homo}}(\tau), \tau + \tau_0)\, d\tau. \tag{42}$$

Melnikov's theorem states that simple zeros of the homoclinic Melnikov function correspond to transversal homoclinic orbits to a hyperbolic fixed point of the two-dimensional Poincaré map existence. Hence chaotic dynamics of the Smale horseshoe type occur for the UEV.

4.4. The subharmonic and homoclinic Melnikov function calculations and their physical interpretation

We now describe how each perturbation influences the UEV motion through the use of the subharmonic and homoclinic Melnikov theories. The three perturbations given in (29) are classified into two categories depending on how they influence the parts of excess kinetic energy. The perturbation in $\sigma(\tau)$, for fixed $\alpha = \alpha_0$, excites $H_S(I, \varphi; \sigma_0, \alpha_0)$ time periodically. Similarly, the perturbation in $\kappa(\tau)$ excites $H_R(I; \kappa_0)$ time periodically. We say that the perturbation is a Hamiltonian perturbation of type 1 (external perturbation) if the time periodic perturbation in the parameter causes a time periodic excitation of a part of the Hamiltonian. The perturbations in $\sigma(\tau)$ and $\kappa(\tau)$ are of this type as can be written as follows:

$$\begin{aligned} H_S(I, \varphi; \sigma(\tau), \alpha_0) &= \{1 + \varepsilon_\sigma \sin \Omega(\tau + \tau_\sigma)\} H_S(I, \varphi; \sigma_0, \alpha_0) \\ H_R(I; \kappa(\tau)) &= \{1 + \varepsilon_\kappa \sin \Omega(\tau + \tau_\kappa)\} H_R(I; \kappa_0). \end{aligned} \tag{43}$$

The perturbation in $\alpha(\tau)$ is somewhat different. For a fixed $\sigma = \sigma_0$ it can be rewritten as follows:

$$H_S(I, \varphi; \sigma_0, \alpha(\tau)) = H_S(I, \varphi - 2\varepsilon_\alpha \sin\Omega(\tau + \tau_\alpha); \sigma_0, 0). \tag{44}$$

Thus we see that the perturbation in $\alpha(\tau)$ has the same effect on H_S as the oscillation of the absolute coordinate axis. Generally, it can be viewed as if the origin of one of canonical variables (in this case

φ) is perturbed around some fixed value time periodically. We call this type of perturbation the Hamiltonian perturbation of type 2 (internal perturbation).

The forms of the Melnikov functions for both types of Hamiltonian perturbations in general provide physical interpretations regarding how the perturbations influence the dynamics (Ide, 1990). Next, we describe the consequences of each type of perturbation, i.e., $\sigma(\tau)$, $\alpha(\tau)$ and $\kappa(\tau)$, and interpret the mathematical results in terms of UEV motion.

4.4.1. Perturbation in $\sigma(\tau)$

On RB $m/1$

The Melnikov function $M_\sigma^{m/n}(\tau_0; \sigma_0, \kappa_0; \Omega)$ for $\varepsilon_\alpha = \varepsilon_\kappa = 0$ is written as follows for the Hamiltonian perturbation of type 1:

$$M_\sigma^{m/n}(\tau_0; \sigma_0, \kappa_0; \Omega) = F_\sigma^{m/n}(\sigma_0, \kappa_0; \Omega) \cos \Omega(\tau_0 + \tau_\sigma) \tag{45}$$

$$F_\sigma^{m/n}(\sigma_0, \kappa_0; \Omega) = \begin{cases} \displaystyle\int_{-mT/2}^{mT/2} \left\{ \frac{\mathrm{d}}{\mathrm{d}\tau} H_S(I, \varphi; \sigma_0, \kappa_0) \right\} \sin \Omega\tau \, \mathrm{d}\tau, & \text{if } n = 1, \\ 0, & \text{if } n \neq 1, \end{cases} \tag{46}$$

where the integrals are evaluated on the corresponding invariant circle having the resonance relation $n\Omega = m\Omega^H$. $M_\sigma^{m/n}(\tau_0; \sigma_0, \kappa_0; \Omega)$ is identically zero for $n \neq 1$, (Ide, 1990). The Melnikov function $M_\sigma^{m/1}(\tau_0; \sigma_0, \kappa_0; \Omega)$ is related to the Fourier transform of the rate of change in the excess kinetic energy induced by the *steady* external straining effect. This is true for both subharmonic and homoclinic Melnikov functions, subject to any one or more of three periodic perturbations. If we know the UEV motion in the steady external linear flow field and how the straining effect contributes to the motion, then we also know how the UEV receives the influence of the perturbation in $\sigma(\tau)$ for a given perturbation frequency Ω through the Melnikov function. From (45), $M_\sigma^{m/1}(\tau_0; \sigma_0, \kappa_0; \Omega)$ has simple zeroes if $F_\sigma^{m/1}(\sigma_0, \kappa_0; \Omega)$ is not identically zero, which guarantees the existence of RB $m/1$. It is clear from the form of the Melnikov function and the graph of $(\mathrm{d}/\mathrm{d}\tau)H_S$ as shown in Fig. 6 that, on a given orbit of Ω^H, the amplitude of $F_\sigma^{m/1}(\sigma_0, \kappa_0; \Omega)$ with $\Omega = m\Omega^H$ is the largest for $m = 1$ because $(\mathrm{d}/\mathrm{d}\tau)H_S$ is more naturally 'synchronized with' $\sin \Omega\tau$ than $\sin \Omega m\tau$ for $m \geqslant 2$. Fig. 9 shows the relation between the signed width of RB $m/1$ up to first order in ε (i.e., $F^{m/1}(\sigma_0, \kappa_0; \Omega) / \| DH_0(q^H(-\tau_0)) \|$), which is on the horizontal axis, and the position of the band on the ζ-axis, which is on the vertical axis.

Each figure shows the three types of perturbations for $(\kappa_0, \sigma_0) = (0.05, -0.25)$ in region 15^+ in Fig. 3 for $m = 1$. This is a typical type of phase portrait in that it contains IHO, OHO, (c-c) and (c) periodic orbits. $F^{m/1}(\sigma_0, \kappa_0; \Omega)$ with $m > 1$ basically show the same type of behavior but much smaller amplitude. In Fig. 9, the solid, broken and one-dot curves correspond to the perturbation in $\sigma(\tau)$, $\alpha(\tau)$ and $\kappa(\tau)$, respectively. On the vertical axis, the position of q_e (elliptic fixed point) is marked by a circle, the positions corresponding to PBO (periodic boundary orbit which governs the transition dynamics) are marked by a asterisk, and the positions corresponding to homoclinic orbits or q_h (hyperbolic fixed point) are marked by a triangle, so as to recognize the original phase space structure shown in Fig. 4.

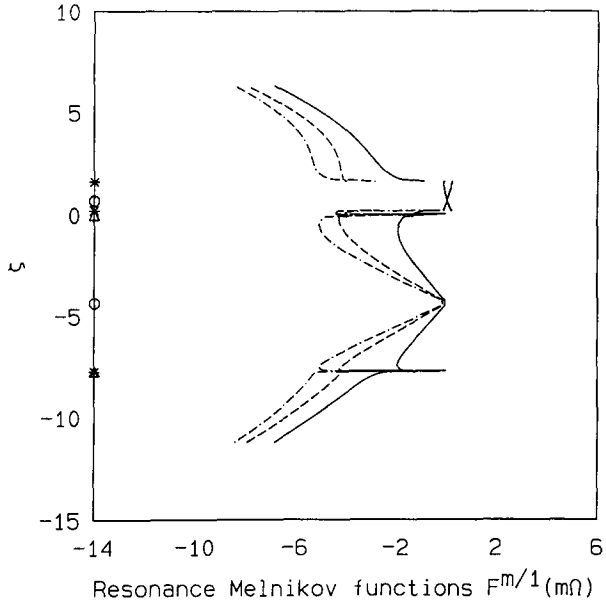

Fig. 9. The width of $RB^{m/1}$ for $m = 1$ for $(\kappa_0, \sigma_0) = (0.05, -0.25)$. $\tau_0 = 0.0500$, $\kappa_0 = -0.2500$, $m = 1$. ——— $F_\sigma^{m/n}(m\Omega)$; – – – $F_\alpha^{m/1}(m\Omega)$; · – · – · – $F_\kappa^{m/n}(m\Omega)$.

On homoclinic orbit

The Melnikov function $M_\sigma(\tau_0; \sigma_0, \kappa_0; \Omega)$ for $\varepsilon_\alpha = \varepsilon_\kappa = 0$ (i.e., the perturbation imposed only on the strength of the straining effect $\sigma(\tau)$) is written as follows:

$$M_\sigma(\tau_0; \sigma_0, \kappa_0; \Omega) = F_\sigma(\sigma_0, \kappa_0; \Omega) \cos \Omega(\tau_0 + \tau_\sigma), \tag{47}$$

with

$$F_\sigma(\sigma_0, \kappa_0; \Omega) = \int_{-\infty}^{\infty} \left\{ \frac{\mathrm{d}}{\mathrm{d}\tau} H_S(I, \varphi; \sigma_0, \kappa_0) \right\} \sin \Omega\tau \, \mathrm{d}\tau, \tag{48}$$

where the integrals are evaluated on the corresponding unperturbed homoclinic orbit. The existence of transversal homoclinic points is guaranteed for $F_\sigma(\sigma_0, \kappa_0; \Omega) \neq 0$. $F_\sigma(\sigma_0, \kappa_0; \Omega)$ is similar to $M_\sigma(\tau_0; \sigma_0, \kappa_0; \Omega)$ without phase shift τ_σ and parametrization variable τ_0. In other words, if we know the UEV motion in the steady external linear flow field and how the straining effect contributes to the motion, then we can determine how the UEV motion is affected by the perturbation in $\sigma(\tau)$, for a given perturbation frequency Ω, through the Melnikov function. If the perturbation is imposed so that it is 'synchronized with' $(\mathrm{d}/\mathrm{d}\tau)H_S$ as the UEV evolves along the homoclinic orbit, then the UEV motion becomes more chaotic.

Earlier we examined how the excess kinetic energy induced by the straining effect (H_S) changes in time for several types of the UEV motion in various (κ_0, σ_0). On the IHO, typically $|(\mathrm{d}/\mathrm{d}\tau) H_S|$ increases in time, attains a local and global maximum, and decays exponentially as $\tau \to \infty$ due to the existence of the hyperbolic fixed point. Hence, for both IHO and OHO in any region of Fig. 3 that possesses homoclinic orbits, the typical behavior of the graph of $F_\sigma(\sigma_0, \kappa_0; \Omega)$ with respect to

Ω is generally as shown in Fig. 10. In this figure we plot the amplitudes of the Melnikov functions corresponding to the three different types of perturbations for $(\sigma, \kappa) = (0.05, -0.25)$ corresponding to region 15^+ in Fig. 3. This phase portrait contains both IHO and OHO. It is a standard result (see, e.g., Wiggins 1990) that the subharmonic Melnikov function converges to the homoclinic Melnikov function as $m \to \infty$.

$|F_\sigma(\sigma_0, \kappa_0; \Omega)|$ increases linearly for Ω small, attains local and global maxima at some frequency (Ω_σ^e), and decays exponentially as $\Omega \to \infty$. We call the frequency which gives the global maximum of the $F_\sigma(\sigma_0, \kappa_0; \Omega)$ the extremum frequency and denote it by Ω_σ^e. The amplitude of $F_\sigma(\sigma_0, \kappa_0; \Omega)$ sensitively depends on Ω.

As we will see later in this section, the Melnikov functions for perturbations in $\kappa(\tau)$ and $\alpha(\tau)$ show the same type of behavior which can be explained by the vortex-energy arguments given in section 3.2.

4.4.2. Perturbation in $\kappa(\tau)$

On RB $m/1$

The Melnikov function $M_\kappa^{m/1}(\tau_0; \sigma_0, \kappa_0; \Omega)$ for $\varepsilon_\kappa = \varepsilon_\alpha = 0$ is written as follows:

$$M_\kappa^{m/n}(\tau_0; \sigma_0, \kappa_0; \Omega) = F_\kappa^{m/n}(\sigma_0, \kappa_0; \Omega) \cos \Omega(\tau_0 + \tau_\kappa), \tag{49}$$

with

$$F_\kappa^{m/n}(\sigma_0, \kappa_0; \Omega) = \begin{cases} \displaystyle\int_{-mT/2}^{mT/2} \left\{ \frac{\mathrm{d}}{\mathrm{d}\tau} H_R(I, \varphi; \sigma_0, \kappa_0) \right\} \sin \Omega\tau \, \mathrm{d}\tau, & \text{if } n = 1, \\ 0, & \text{if } n \neq 1, \end{cases} \tag{50}$$

where the integrals are evaluated on the corresponding invariant circle with the resonance relation $n\Omega = m\Omega^H$ and Ω^H of the natural frequency of the unperturbed orbit. Due to the symmetry, $M_\kappa^{m/n}(\tau_0; \sigma_0, \kappa_0; \Omega)$ for $n \neq 1$ is identically zero and the existence of RB $m/1$ is guaranteed for $F_\kappa^{m/1}(\sigma_0, \kappa_0; \Omega) \neq 0$. Again the knowledge of H_R during UEV evolution in the basic steady external linear flow field provides the information regarding the dynamics in the unsteady $\kappa(\tau)$ field. The behavior of $F_\kappa^{m/1}(\sigma_0, \kappa_0; \Omega)$ is quite similar to that of $F_\sigma^{m/1}(\sigma_0, \kappa_0; \Omega)$.

On homoclinic orbit

Since the perturbation in $\kappa(\tau)$ excites H_R time periodically as the perturbation in $\sigma(\tau)$ excites H_S time periodically, we now examine the influence of the perturbation in the strength of the background vorticity effect on the UEV dynamics by examining the Melnikov function as we did for the perturbation in $\sigma(\tau)$. The Melnikov function $M_\kappa(\tau_0; \sigma_0, \kappa_0; \Omega)$ for $\varepsilon_\sigma = \varepsilon_\alpha = 0$ (i.e., the perturbation imposed only on the strength of the straining effect $\kappa(\tau)$) is written as follows:

$$M_\kappa(\tau_0; \sigma_0, \kappa_0; \Omega) = F_\kappa(\tau_0; \sigma_0, \kappa_0; \Omega) \cos \Omega(\tau_0 + \tau_\kappa), \tag{51}$$

with

$$F_\kappa(\sigma_0, \kappa_0; \Omega) = \int_{-\infty}^{\infty} \left\{ \frac{\mathrm{d}}{\mathrm{d}\tau} H_R(I, \varphi; \sigma_0, \kappa_0) \right\} \sin \Omega\tau \, \mathrm{d}\tau, \tag{52}$$

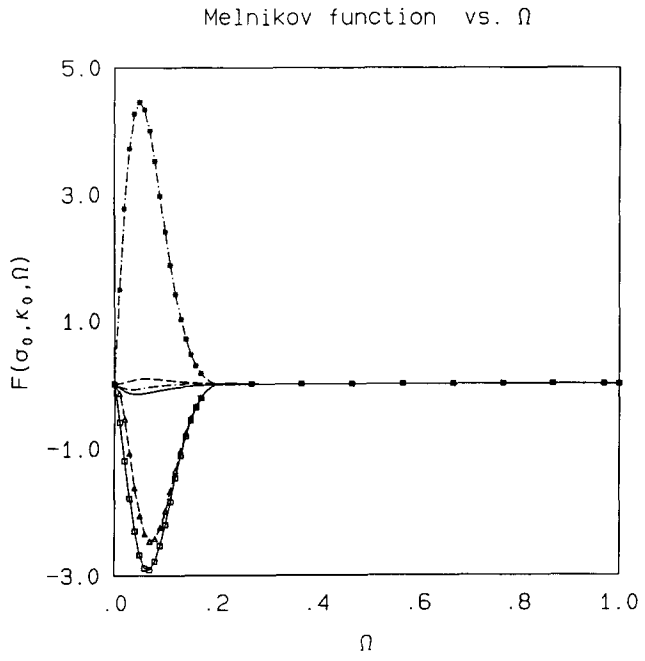

Fig. 10. The Graph of $F(\sigma_0, \kappa_0; \Omega)$ versus Ω for $(\sigma, \kappa) = (0.05, -0.25)$. $\tau_0 = 0.0500$, $\kappa_0 = -0.2500$, $m = 1$. Inner homoclinic orbot ——— $F_\sigma(\sigma_0, \kappa_0; \Omega\sigma)$; – – – $F_\alpha(\sigma_0, \kappa_0; \Omega\alpha)$; · · · · · $F_\kappa(\sigma_0, \kappa_0; \Omega\kappa)$. Outer homoclinic orbot. □–·–·–□ $F_\sigma(\sigma_0, \kappa_0; \Omega)$ △–·–·–△ $F_\alpha(\sigma_0, \kappa_0; \Omega\alpha)$; ■–·–·–■ $F_\kappa(\sigma_0, \kappa_0; \Omega\kappa)$.

where the integrals are evaluated on the corresponding unperturbed homoclinic orbit. The existence of the transversal homoclinic points is guaranteed for $F_\kappa(\sigma_0, \kappa_0; \Omega) \neq 0$. The physical interpretation of $F_\kappa(\tau_0; \sigma_0, \kappa_0; \Omega)$ is similar to that for $F_\kappa^{m/1}(\tau_0; \sigma_0, \kappa_0; \Omega)$ and its behavior is similar to $F_\sigma(\tau_0; \sigma_0, \kappa_0; \Omega)$ as shown in Fig. 10.

4.4.3. Perturbation in $\alpha(\tau)$

On RB m/n

The Melnikov function $M_\alpha^{m/n}(\tau_0; \sigma_0, \kappa_0; \Omega)$ for $\varepsilon_\sigma = \varepsilon_\kappa = 0$ is written as follows.

$$M_\alpha^{m/n}(\tau_0; \sigma_0, \kappa_0; \Omega) = F_\alpha^{m/n}(\sigma_0, \kappa_0; \Omega) \sin \Omega(\tau_0 + \tau_\alpha), \tag{53}$$

$$F_\alpha^{m/n}(\sigma_0, \kappa_0; \Omega) = \begin{cases} \displaystyle\int_{-mT/2}^{mT/2} \left\{ \frac{d^2}{d\tau^2} I \right\} \cos \Omega\tau \, d\tau, & \text{if } n = 1, \\ 0, & \text{if } n \neq 1, \end{cases} \tag{54}$$

where the integrals are evaluated on the corresponding invariant circle with the resonance relation $m\Omega^H = n\Omega$. If we know the UEV motion in the steady external linear flow field and how the angular momentum of the UEV changes, then we also know how the UEV motion is influenced by the perturbation.

On homoclinic orbit

The Melnikov function $M_\alpha(\tau_0; \sigma_0, \kappa_0; \Omega)$ for $\varepsilon_\sigma = \varepsilon_\kappa = 0$ (i.e., the perturbation imposed only on the inclination angle of the straining axis $\alpha(\tau)$) is written as follows because the perturbation is a Hamiltonian perturbation of type 2:

$$M_\alpha(\tau_0; \sigma_0, \kappa_0; \Omega) = F_\alpha(\sigma_0, \kappa_0; \Omega) \sin \Omega(\tau_0 + \tau_\alpha) \tag{55}$$

with

$$F_\alpha(\sigma_0, \kappa_0; \Omega) = \int_{-\infty}^{\infty} \left\{ \frac{d^2}{d\tau^2} I \right\} \cos \Omega\tau \, d\tau, \tag{56}$$

where the integrals are evaluated on the corresponding unperturbed homoclinic orbit. The existence of the transversal homoclinic points is guaranteed for $F_\alpha(\sigma_0, \kappa_0; \Omega) \neq 0$. $F_\alpha(\sigma_0, \kappa_0; \Omega)$ is similar to $M_\alpha(\tau_0; \sigma_0, \kappa_0; \Omega)$ without phase shift τ_α and parametrization variable τ_0.

4.4.4. Relationships between the different types of Perturbations and the role and influence of parameters

Since the total kinetic energy is conserved in the flow field, there are certain relations amongst the functions F and $F^{m/1}$'s that we discuss in this section. The arguments heavily rely on the energetics of the UEV which we discussed in section 3.2.

(i) From (24), the following relation holds both for subharmonic and homoclinic Melnikov functions:

$$F_E(\sigma_0, \kappa_0; \Omega) = F_\sigma(\sigma_0, \kappa_0; \Omega) + F_\kappa(\sigma_0, \kappa_0; \Omega),$$

where

$$F_E(\sigma_0, \kappa_0; \Omega) = \int_{-T^*}^{T^*} \left\{ \frac{d}{d\tau} H_E(I, \varphi; \sigma_0, \kappa_0) \right\} \sin \Omega\tau \, d\tau,$$

$$T^* = \begin{cases} mT/2 & \text{on RB } m/1, \\ \infty, & \text{on homoclinic orbits,} \end{cases} \tag{57}$$

and the integral is evaluated on the appropriate unperturbed orbit. $F_E(\sigma_0, \kappa_0; \Omega)$ corresponds to the Fourier transform of the rate of change in the self-induced excess kinetic energy. On the homoclinic orbits using the previous discussion, the graph of $F_E(\sigma_0, \kappa_0; \Omega)$ typically behaves like other F's with respect to Ω. Since the level sets for $H_E(I)$ and $H_R(I)$ are both circular in $\delta - \zeta$ space, the extremum frequency for $F_E(\sigma_0, \kappa_0; \Omega)$ is of the same order as $F_\kappa(\sigma_0, \kappa_0; \Omega)$. It follows from the above equation that the extremum frequencies for $F_\sigma(\sigma_0, \kappa_0; \Omega)$ and $F_\kappa(\sigma_0, \kappa_0; \Omega)$ are of the same order, i.e.,

$$\Omega_\sigma^e \sim \Omega_\kappa^e.$$

(ii) $F_\alpha(\sigma_0, \kappa_0; \Omega)$ and $F_\kappa(\sigma_0, \kappa_0; \Omega)$ have the following relationship:

$$-\kappa_0 F_\alpha(\sigma_0, \kappa_0; \Omega) = \Omega F_\kappa(\sigma_0, \kappa_0; \Omega). \tag{58}$$

For a given (κ_0, σ_0), the ratio of values of $F_\alpha(\sigma_0, \kappa_0; \Omega)$ and $F_\sigma(\sigma_0, \kappa_0; \Omega)$ is proportional to the perturbation frequency Ω. From Eq. (58) and the behavior of $F_\alpha(\sigma_0, \kappa_0; \Omega)$ and $F_\kappa(\sigma_0, \kappa_0; \Omega)$, it can be shown that the following relation holds:

$$\Omega_\alpha^e < \Omega_\kappa^e. \tag{59}$$

Region in (κ_0, σ_0)	Some typical UEV motion and mechanisms
1	• (C-C) osc on $RB\ \frac{m}{1}$, KAM, *can* • transition between (C-C) osc. and rot if $RB\ \frac{m}{1}$ includes the origin of (δ, ζ) • (C-C) osc on $RB^m{}_T$, KAM, *can*
3	• (C-C) osc on $RB\ \frac{m}{1}$, KAM, *can* • transition between (C-C) osc. and rot if $LRB\ \frac{m}{1}$ includes the origin of (δ, ζ) • (C-C) osc on $RB\ \frac{m}{1}$, KAM, *can* • transition between (C-C) rot. and irreversible elongation through homoclinic tangles • chaotic (C-C) rot. along horseshoe map
near 4	• (C-C) osc on $RB\ \frac{m}{1}$, KAM, *can* • transition between (C-C) osc. and irreversible elongation through homoclinic tangles • chaotic (C-C) osc and rot. along horseshoe map
5	• (C-C) osc on $RB\ \frac{m}{1}$, KAM, *can* • transition between (C-C) osc. and irreversible elongation through homoclinic tangles • chaotic (C-C) osc. along horseshoe map
13	• (C-C) osc on $RB\ \frac{m}{1}$, KAM, *can* • transition between (C-C) osc. and rot if $RB\ \frac{m}{1}$ includes the origin of (δ, ζ) • (C-C) osc on $RB\ \frac{m}{1}$, KAM, *can* • (C) osc on $RB\ \frac{m}{1}$, KAM, *can* • (C) rot on $RB\ \frac{m}{1}$, KAM, *can* • transition between (C-C) rot, (C) osc, and (C) rot. through inner and outer homoclinic tangles • chaotic (C-C) osc, (C) osc., and (C) rot along horseshoe map
14	• (C-C) osc on $RB\ \frac{m}{1}$, KAM, *can* • (C-C) osc on $RB\ \frac{m}{1}$, KAM, *can* • transition between (C-C) osc., (C) osc., and (C) rot. through inner and outer homoclinic tangles • chaotic (C-C) osc., (C) osc., and (C) rot. along horseshoe map
15	• (C-C) osc on $RB\ \frac{m}{1}$, KAM, *can* • (C) osc on $RB\ \frac{m}{1}$, KAM, *can* • transition between (C-C) osc. and (C) rot. if $RB\ \frac{m}{1}$ includes the origin of (δ, ζ) • (C) rot on $RB\ \frac{m}{1}$, KAM, *can* • transition between (C-C) osc. and (C) rot. through inner and outer homoclinic tangles • chaotic (C-C) osc. and (C) rot. along horseshoe map
17	• (C) osc. on $RB\ \frac{m}{1}$, KAM, *can* • transition between (C) rot. and (C) rot. if $RB\ \frac{m}{1}$ includes the origin of (δ, ζ) • (C) rot on $RB^m{}_T$, KAM, *can*

Fig. 11. Typical UEV motions in the time-periodic linear external field, and the mechanisms that give rise to these motions.

(iii) Let us consider the effect of varying the parameters (κ_0, σ_0) on the extremum frequencies for the different types of perturbations. In general, the extremum frequency Ω^e depends on how fast the orbit approaches the hyperbolic fixed point q_h. Hence, Ω^e sensitively depends on the eigenvalues at q_h and the elliptic fixed point on the positive ζ-axis (q_e^+) for IHO. For OHO, Ω^e depends on the eigenvalues at q_h and the elliptic fixed point on the negative ζ-axis (q_e^-), and the natural frequency at $I \to \infty$. It follows that $\Omega^e \to 0$ for (κ_0, σ_0) near bifurcation values on the bifurcation curves S^+, R and I_1^+ for IHO, and S^+ and R for OHO.

(iv) The effect of varying the parameters (κ_0, σ_0) on the amplitude of the F's can be also given by the phase space structure and the UEV energetics. It is clear from the form of the F's that the amplitude of the F's that the amplitude of the F's is larger when $\mathrm{d}I/\mathrm{d}\tau$ on the corresponding orbit is larger. Recall also that the IHO disappears to infinity for (κ_0, σ_0) close to I_1^+, which implies that the amplitude of the F's also grows.

4.5. Summary of the qualitatively different types of UEV motion in time-periodic external linear flow fields

In Fig. 11 we summarize the qualitatively different types of UEV motion in time periodic linear external flow field corresponding to values of (κ_0, σ_0) in the regions in Fig. 3 denoted by 1^+, 3^+, 4^+, 5^+, 13^+, 14^+, 15^+ and 17^+. In this figure *KAM* denotes the abbreviation for a "KAM torus" and *can* is an abbreviation for "cantorus".

5. Summary

Isolated concentrations of vorticity are commonly observed in a variety of almost two-dimensional, incompressible, inviscid flows. Such vortices appear to be persistent and often are characterized by an elliptical configuration with time varying aspect ratio and inclination angle. A system of UEV's in a linear external field is a first order approximation to the model motion of an isolated vortex or interaction processes among isolated vortices in a Lagrangian frame moving with one of the vortices.

A Hamiltonian formulation, in which one of the two variables for the UEV motion and the Hamiltonian represent the UEV angular momentum and excessive kinetic energy of the total flow field, respectively, was derived. The Hamiltonian has three components; one due to self-induced motion, the other two due to strain and rotation of the external flow field. The system thus describes how the UEV and the external flow exchange angular momentum and energy during the evolution, which provides physical insight into general vortex-interaction processes.

When the external linear flow field is time independent, all possible UEV motions can be compactly described by a phase plane diagram, or *phase portrait*, for a given flow parameter set. The phase space is divided into several regions that correspond to different types of regular UEV motion; steady state, oscillation, rotation, asymptotic approach to a steady state, and elongation. The boundaries between these regions are defined by IHO, OHO, periodic orbits passing through the origin of the coordinate system, and unbounded invariant manifolds emanating from the hyperbolic fixed point. In the parameter space, regions of qualitatively different phase-portrait structure are separated by bifurcation curves.

New types of motion become possible in time-periodically varying external linear flows. A UEV can undergo either regular or irregular motion, and change its type of motion during the evolution. Mechanisms for chaotic transition are provided by homoclinic tangles and resonance bands, while quasi-periodic UEV motion is explained by the existence of the KAM tori. The Melnikov technique not only predicts such motions qualitatively but also gives quantitative information including the UEV response to perturbation type and frequency.

References

Batchelor, G.K. (1954) *An Introduction to Fluid Dynamics*, (Cambridge University Press).

Bertozzi, A. (1988) Heteroclinic Orbits and Chaotic Dynamics in Planar Fluid Flows, *SIAM J. Math. Anal. 19*, 1271–1294.

Ide, K. (1990) Ph.D. thesis. California Institute of Technology.

Jimenez, J. (1987) On the Linear Stability of the Inviscid Kármán Vortex Street, *Fluid Mechanics 178*, 177–194.

Kirchoff, G. (1876) Mechanik, Leipzig.

Kida, S. (1981) Motion of an Elliptical Vortex in a Uniform Shear Flow, *J. Phys. Soc. Japan, 50*, 3517–3520.

Lamb, S.H. (1932) *Hydrodynamics*, 6th Ed. (Cambridge University Press).

McWilliams, J.C. (1984) The Emergence of Isolated Coherent Vortices in Turbulent Flow, *J. Fluid Mechanics 140*, 21–43.

Melander, M.V., N.J. Zabusky, and S. Styczek (1987) A Moment Model for Vortex Interactions of the Two-Dimensional Euler Equations: Part I. Computation of a Hamiltonian elliptical Representation *J. Fluid Mechanics 167*, 95–115.

Moore, D.W. and P.G. Saffman (1971) *Structure of a Line Vortex in an Imposed Strain. Aircraft Wake Turbulence and Its Detection* (Plenum Press) 339–354.

Moore, D.W. and P.G. Saffman (1975) The Density of Organized Vortices in a Turbulent Mixing Layer *J. Fluid Mechanics 69*, 465–473.

Neu, J.C. (1984) The Dynamics of a Columnar Vortex in an Imposed Strain, *Physics Fluids 27*, 2397–2402.

Rom-Kedar, V.A. Leonard and S. Wiggins (1989) An Analytical Study of Transport, Mixing and Chaos in an unsteady Vortical Flow, *J. Fluid Mechanics 214*, 347–394.

Roshko, A. (1976) Structure of Turbulent Shear Flows: A New Look, *AIAA Journal 14*, 1849–1857.

Saffman, P.G. and J.C. Schatzman (1982) Stability of a Vortex Street of Finite Vortices. *J. Fluid Mechanics 117*, 171–185.

Saffman, P.G. and G.R. Baker (1979) Vortex Interactions, *Annual Review Fluid Mechanics 11*, 95–112.

Wiggins, S. (1990) *Introduction to Applied Nonlinear Dynamical Systems and Chaos* (Springer, Berlin).

Wiggins, S. (1992) *Chaotic Transport in Dynamical Systems (Springer Berlin)*.